PHYSICAL REVIEW D **88,** 103505 (2013)

Nonlinear power spectra of dark and luminous matter in the halo model of structure formation

Yurij Kulinich,* Bohdan Novosyadlyj,† and Stepan Apunevych‡

Astronomical Observatory of Ivan Franko National University of Lviv, Kyryla i Methodia strasse, 8, Lviv 79005, Ukraine

(Received 23 March 2012; published 7 November 2013)

The late stages of large-scale structure evolution are treated semianalytically within the framework of the modified halo model. We suggest a simple yet accurate approximation for relating the nonlinear amplitude to the linear one for spherical density perturbation. For halo concentration parameter c, a new computation technique is proposed, which eliminates the need for interim evaluation of the $z_{\rm col}$. The validity of the technique is proved for ΛCDM and ΛWDM cosmologies. Also, the parameters for the Sheth-Tormen mass function are estimated. The modified and extended halo model is applied for determination of the nonlinear power spectrum of dark matter, as well as for a galaxy power spectrum estimation. The semianalytical techniques for the dark matter power spectrum are verified by comparison with data from numerical simulations. Also, the predictions for the galaxy power spectra are confronted with ''observed'' data from the Infrared Astronomical Satellite Point Source Catalog Redshift Survey (PSCz) and Sloan Digital Sky Survey (SDSS) galaxy catalogs, good accordance is found.

DOI: 10.1103/PhysRevD.88.103505 PACS numbers: 98.80.−k, 98.65.−r, 95.35.+d

I. INTRODUCTION

A commonly accepted inflationary paradigm states that the large-scale structure of the Universe is formed through evolution of density perturbations driven by gravitational instability. At some moment, the growth of small-scale perturbations switches to the nonlinear regime. The treatment of the linear regime is quite simple; the linear power spectrum (transfer function) for $k < 0.1$ h/Mpc can be readily computed with percent accuracy for any feasible cosmology. However, it is not so for the smaller scales, due to the nonlinear terms in equations and the complexity of physics of the baryonic component (hydrodynamics, radiation transfer, and thermal and chemical evolution). This paper is aimed for the development of a technique capable to build a bridge between the initial (linear) matter power spectrum and the observable (inherently nonlinear) galaxy power spectrum. The treatment is based on the halo model complemented by analytical approximations, and the results are tested and verified against the data of N-body simulations.

Within the scenario commonly referred as ''standard'' (see [1]), the gravitational potential of collisionless dark matter inhomogeneities governs the baryonic matter until the baryonic matter power spectrum reaches the dark matter one in amplitude. At some moment, a nonlinear perturbation with amplitude exceeding some critical one detaches from background expansion, reaches a turnaround point, and starts to collapse due to self-gravity. Subsequently, a violent relaxation takes place, which brings the system into virial equilibrium, so the halo of dark matter is formed. Then, the baryonic gas starts to cool down, followed by clumping into clouds and ignition of the luminous tracers within halos (see [2,3] for details).

Thus, the spatial distribution of luminous matter should strongly correlate with one of the halos. The correlation is confirmed by large simulations, which take into account the baryon physics and particle dynamics of dark matter [4,5], and by semianalytic models of galaxy formation [6–8] as well. The numerical techniques require considerable computing power, whereas the purely analytical are found to be unreliable and inaccurate. Thus, the ''hybrid'' approach seems to be optimal, combining the analytical model of galaxy formation [9,10] with dark matter ''merger trees'' extracted from simulations. Another way is to extract the halo and subhalo statistics from simulations for comparison with galaxy populations in a large galaxy survey. Such techniques are based on the conditional luminosity function (CLF) [11–13], conditional mass function (CMF) [14], and stellar mass to halo mass relation [14,15].

The halo model is a cornerstone of the modern theory of structure formation. It has been proven to be well motivated and comprehensive and provides a plausible explanation for observational data and results of cosmological simulations. It is valid for a wide range of cosmologies, as long as the statistics of primordial density perturbations is Gaussian. It encompasses the nonlinear stage of the evolution of density perturbations as well as the dynamical relaxation processes assuming that the whole mass is associated with a gravitationally bound virialized halo.

It has shown in Refs. [16–18] that the dark matter nonlinear power spectrum can be evaluated given halo statistics, their internal structure, and spatial distribution. Also, *vice versa*, the initial power spectrum can be reconstructed by applying the halo model to the data of N-body simulations. As another example, the halo occupation function $p(N|M)$, the probability of finding N galaxies within a halo of mass M, was used in Refs. [19,20] along with the halo model to calculate the nonlinear galaxy power spectrum. However, regardless of the overall

*kul@astro.franko.lviv.ua
†novos@astro.franko.lviv.ua
‡apus@astro.franko.lviv.ua

success of the halo model[1] in a description of dark matter and galaxy clustering, it is still not to be considered as complete. For instance, only the latest enhancements proposed in [22,23] take into account the internal structure of the halo as well as the halo shapes [24,25].

To apply the halo model, the *a priori* knowledge of the evolution of inhomogeneities from the initial state through collapse to the formation of a virialized halo is required. In Sec. II, we analyze such an evolution by using the spherical perturbation model in order to analytically relate the amplitude of the nonlinear spherical density perturbation to that of the linear. Also, a new technique is proposed therein for computation of concentration parameter c for a halo with a Navarro-Frenk-White (NFW) density profile. In Sec. III, the halo mass function is applied to dark matter clustering. In Sec. IV, the galaxy power spectra are estimated and compared to observable ones, as derived in Refs. [26,27] from the Infrared Astronomical Satellite Point Source Catalog Redshift Survey (PSCz) and Sloan Digital Sky Survey (SDSS) catalogs. The conclusions are presented in Sec. V. The computations were performed for the ΛCDM (cold dark matter with the Λ term) and ΛWDM (warm dark matter with the Λ term) cosmological models, and some bulk mathematical derivations are separated in Appendixes.

II. FORMATION OF INDIVIDUAL SPHERICAL HALO

A. Spherical overdensity with arbitrary profile

In the framework of Tolman's approach [28], the spherically symmetrical inhomogeneity is treated in the synchronous gauge (i.e. with regard to the frame comoving to the dustlike matter component), with space-time interval

$$ds^2 = dt^2 - \frac{y^2(t,R)}{\sqrt{1-KR^2}}dR^2 - x^2(t,R)R^2(d\theta^2 + \sin^2\theta d\varphi^2), \quad (1)$$

where t is the proper time of an observer located at R and K is space curvature of the Universe as the whole. For a homogeneous Friedmann universe, $x(t) = y(t) = a(t)$.

The mean matter density, i.e. average value over a sphere of radius R, is denoted by $\rho_M(\tau,R) \equiv \rho_m^0 x^{-3}(\tau,R)$, and the matter density at some specific distance R from the center of perturbation is $\rho(\tau,R) \equiv \rho_m^0 x^{-2}(\tau,R)y^{-1}(\tau,R)$; see [29,30] for details. Let us define the amplitude of density perturbation as follows:

$$\delta_\rho(t,R) = \frac{\rho(t,R)-\bar\rho(t)}{\bar\rho(t)} = \frac{a^3(t)}{x^2(t,R)y(t,R)} - 1, \quad (2)$$

and the amplitude of the mass perturbation is

$$\delta_M(t,R) = \frac{\rho_M(t,R)-\bar\rho(t)}{\bar\rho(t)} = \frac{a^3(t)}{x^3(t,R)} - 1. \quad (3)$$

[1]The details of the halo model can be found in [21].

These amplitudes (see [29]) are related by

$$\delta_M(t,R) = \frac{3}{r^3(t,R)}\int_0^R \delta_\rho(t,R)r^2(t,R)r'(t,R)dR \quad (4)$$

with $r(t,R) = x(t,R)R$, $(') \equiv d/dR$.

For small perturbations, the following approximations are valid for (2) and (3):

$$\delta_\rho(t,R) \simeq \delta(t,R) \equiv A(R)D(a(t)) \ll 1, \quad (5)$$

$$\delta_M(t,R) \simeq \bar\delta(t,R) \equiv \frac{3}{5}\frac{\Omega_K - \Omega_f(R)}{\Omega_m}D(a(t)) \ll 1, \quad (6)$$

where $D(a(\tau))$ is the growth factor of linear matter density perturbations [31,32], defined by

$$D(a) = \frac{5}{2}\Omega_m a^{-1}X^{1/2}(a)\int_0^a X^{-3/2}(\tilde a)d\tilde a, \quad (7)$$

where $X(a) \equiv \Omega_\Lambda a^2 + \Omega_m a^{-1} + \Omega_K$. The parameter of local curvature, $\Omega_f(R)$, can be related due to Eq. (4) with the density profile $A(R)$ from (6) as

$$\Omega_f(R) = -5\Omega_m R^{-3}\int_0^R A(\tilde R)\tilde R^2 d\tilde R + \Omega_K. \quad (8)$$

Thus, either $A(R)$ or $\Omega_f(R)$ should be specified to define the initial profile of perturbation.

Einstein's equations for spherical overdensity of dustlike matter in the model with a cosmological constant, $G_1^1 = G_2^2 = \Lambda$, yield the equations for $x(\tau,R)$ and $y(\tau,R)$:

$$\ddot x = \frac{3}{2}\Omega_\Lambda x - \frac{1}{2}\frac{\dot x^2}{x} + \frac{1}{x}\frac{\Omega_f}{2}, \quad (9)$$

$$\ddot y = \frac{3}{2}\Omega_\Lambda y - \left(\frac{\dot x\,\dot y}{x} - \frac{1}{2}\frac{\dot x^2 y}{x^2}\right) + \left(\Omega_f + R\frac{\Omega_f'}{2}\right)\frac{1}{x} - \frac{y}{x^2}\frac{\Omega_f}{2}. \quad (10)$$

The overdot denotes a derivative with respect to $\tau = H_0 t$. The first integration of (9) yields

$$\dot x^2 - \frac{\Omega_m}{x} - \Omega_\Lambda x^2 = \Omega_f. \quad (11)$$

Thus, the amplitude of mass perturbation, (3), can be calculated by integrating over time just this single equation.

The development of spherical inhomogeneity can be divided into two stages: (i) the expansion stage ($\dot x > 0$, $\dot\rho_M < 0$), linear and weakly nonlinear regime; (ii) the collapse stage ($\dot x < 0$, $\dot\rho_M > 0$), entirely nonlinear regime. They are separated by the moment of turnaround, when $\dot x = 0$ ($\dot\rho_M = 0$).

The evolution of perturbation at the nonlinear stage is convenient to be treated by confrontation with the evolution of some fictitious linear perturbation extrapolated beyond the linear stage. Therefore, the time dependence is represented in terms of the ratio of $\bar\delta$, the initial mean overdensity of linear perturbation at some R, to the $\delta_{\rm col}$,

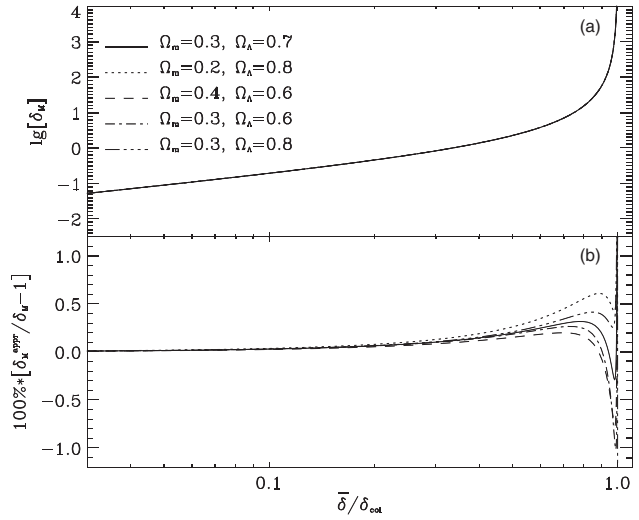

FIG. 1. Top panel: The dependence of the nonlinear amplitude of spherical perturbation on the linear one. Bottom panel: The accuracy of the approximation (12) for some cosmological models, where $\delta_M^{\rm appr}$ denotes the right-hand side of (12) and δ_M is the exact value.

critical overdensity [29,31,33], the amplitude of perturbation which is to collapse at the moment $t_{\rm col}$.

In Fig. 1, the dependence of the nonlinear amplitude on the ratio $\bar{\delta}/\delta_{\rm col}$ is plotted, as computed by integration of Eqs. (10) and (11). The fit for the dependence is simple:

$$\lg[1+\delta_M] \simeq -\delta_{\rm col}\cdot\lg[1-\bar{\delta}/\delta_{\rm col}] + A\cdot\lg^2[1-\bar{\delta}/\delta_{\rm col}] + B\cdot\lg^3[1-\bar{\delta}/\delta_{\rm col}], \quad (12)$$

and the coefficients are $A = 0.0903$ and $B = 0.0074$. This fit is similar to that proposed by Ref. [34], wherein the values $A = 0$ and $B = 0$ were assumed; see also [35]. The fitting errors do not exceed 1% until the moment of complete collapse, when $\delta_M \to \infty$ (bottom panel of Fig. 1).

Given δ_M, the density amplitude δ_ρ is to be evaluated at any radius R with

$$\delta_\rho = \frac{1+\delta_M}{1+(\bar{\delta}-\delta)\frac{\partial}{\partial\delta}\ln(1+\delta_M)} - 1. \quad (13)$$

B. Virialization and final parameters of individual spherical halo

Note that the true singularity at the collapse stage in the center of the overdensity as a rule is not reached, since the falling of particles usually is not strictly radial and small-scale inhomogeneities within the cloud induce the additional nonradial velocities of particles. The process of virialization is far from trivial, however; when the relaxation is finished and dynamical equilibrium is established, the kinetic energy and the gravitational potential satisfy the virial theorem. For instance, for a spherical relaxed halo the kinetic energy per unit mass is determined by

$$T_{\rm vir}/m = \frac{1}{2}\langle v^2\rangle_{\rm vir} = \frac{1}{2}r\frac{\partial U_{\rm vir}}{\partial r}.$$

For the ΛCDM model $U_{\rm vir} = -H_0^2\Omega_\Lambda x_{\rm vir}^2 - H_0^2\Omega_m/x_{\rm vir}$ [31], and the total energy of the isolated dark matter cloud is conserved. By equating the total energy at the turnaround point (kinetic energy is zero and $E_{\rm tot} = U_{\rm ta}$) to the one at the virialization epoch ($E_{\rm tot} = U_{\rm vir} + T_{\rm vir}$), we obtain

$$2\Omega_\Lambda x_{\rm vir}^2 + \frac{1}{2}\frac{\Omega_m}{x_{\rm vir}} = \Omega_\Lambda x_{\rm ta}^2 + \frac{\Omega_m}{x_{\rm ta}}. \quad (14)$$

With Eq. (11) for the turnaround point, $\dot{x}(\tau_{\rm ta}) = 0$, we get the cubic equation for $x_{\rm vir}$:

$$4\Omega_\Lambda x_{\rm vir}^3 + 2\Omega_f x_{\rm vir} + \Omega_m = 0, \quad (15)$$

with a real root for overdensity ($\Omega_f < 0$) in the cosmology with $\Omega_\Lambda > 0$:

$$x_{\rm vir} = \left(-\frac{2\Omega_f}{3\Omega_\Lambda}\right)^{\frac{1}{2}}\cos\left\{\frac{1}{3}\arccos\left[-\frac{\Omega_m}{8\Omega_\Lambda}\left(-\frac{6\Omega_\Lambda}{\Omega_f}\right)^{\frac{3}{2}}\right] - \frac{2\pi}{3}\right\}. \quad (16)$$

For $\Omega_\Lambda = 0$, Eq. (14) implies the strict equality $x_{\rm vir} = x_{\rm ta}/2$. For $\Omega_\Lambda > 0$, $x_{\rm vir} < x_{\rm ta}/2$, albeit the difference is not large. In the fiducial model with $\Omega_\Lambda = 0.7$ and $\Omega_m = 0.3$ for a perturbation collapsing at the current epoch, the relative difference $(\frac{1}{2}x_{\rm ta} - x_{\rm vir})/x_{\rm vir}$ is indeed ∼0.1 and diminishes with either Ω_Λ decrease or increase of the collapse

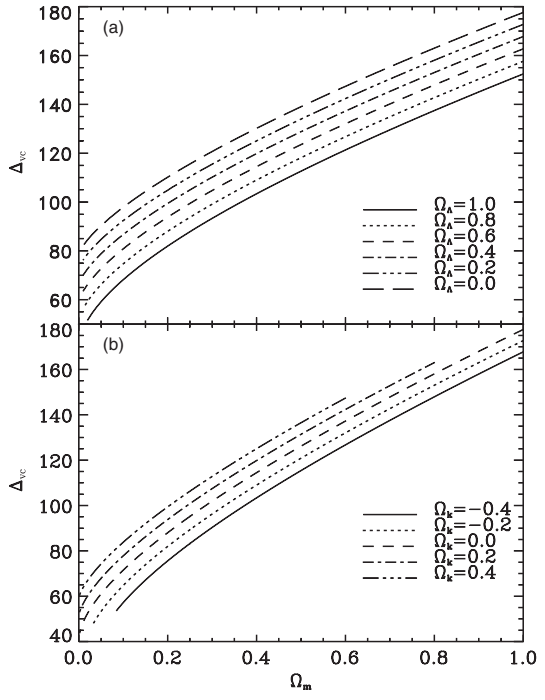

FIG. 2. The dependence of the virialized spherical cloud density on Ω_m in units of the critical density at the moment of collapse, $\Delta_{\rm vc}$, for models with fixed Ω_Λ (a) and Ω_K (b).

redshift. Therefore, the approximation $x_{\rm vir} \approx x_{\rm ta}/2$ can be applied in most cases.

Note that the value of $x_{\rm vir}$ depends on the local curvature Ω_f and consequently on the collapse time $t_{\rm col}$. Also, the virial mass density $\rho_{\rm vir} = \rho_m^0 x_{\rm vir}^{-3}$ depends on $t_{\rm col}$. It is convenient to represent the virial density in units of the critical one, taken at the moment of collapse:

$$\Delta_{\rm vc} = \frac{\rho_{\rm vir}(\tau_{\rm col})}{\rho_{\rm cr}(\tau_{\rm col})} = \frac{\Omega_m H_0^2}{x_{\rm vir}^3(\tau_{\rm col}) H^2(\tau_{\rm col})}. \quad (17)$$

For the Einstein–de Sitter model ($\Omega_m = 1$, $\Omega_\Lambda = 0$), this ratio does not depend on the collapse moment and equals $\Delta_{\rm vc} = 18\pi^2 \simeq 178$. For other cosmologies, e.g. $\Omega_\Lambda \neq 0$ and/or $\Omega_K \neq 0$, the value $\Delta_{\rm vc}$ depends on $\tau_{\rm col}$ and for newly formed halos it is shown in Fig. 2.

III. DENSITY PROFILES AND CONCENTRATION PARAMETER

The basic assumption of the halo model is that dark matter is associated with virialized halos, which have some universal density profile. The halo density profile is described by the generic expression $\rho(r) = \rho_s (r/r_s)^{-\gamma} \times (1 + r/r_s)^{\gamma-\alpha}$, with coefficients restricted by Ref. [36] to $2.5 \leq \alpha \leq 3$ and $1 \leq \gamma \leq 1.5$. The characteristic radius r_s specifies the distance at which the slope of the density profile changes. We use the universal NFW density profile [33] henceforth; this is a special case of the generic profile with the values of the slopes fixed as $\gamma = 1$ and $\alpha = 3$:

$$\rho(r) = \frac{\rho_s}{(r/r_s)(1 + r/r_s)^2}. \quad (18)$$

For this density profile, the total halo mass diverges logarithmically with r, whence the size of each halo has to be limited to some finite value.

The characterization of the halo is a matter of convention. Here, the mass of the halo is defined as the mass of the whole matter contained within the volume of radius $r_{\rm vir}$. The quantity $r_{\rm vir}$ is defined as a radius of the sphere, the mean internal density of which exceeds the value of the critical density by some fixed factor. In the case of the factor 200, the halo mass is denoted by M_{200}; for $\Delta_{\rm vc}$ used as a factor, M_Δ is a denotation of halo mass. Sometimes the factor is assumed to be 180, so that M_{180} is used accordingly. The index is omitted when the choice of definition is clear from the context.

The ratio of radius $r_{\rm vir}$, used for defining the halo, to the quantity r_s is called the concentration parameter (or just concentration) and denoted as c. Depending on the definition of $r_{\rm vir}$, the corresponding index is used as c_{200}, c_Δ, or c_{180}. By defining the mass of the halo and concentration parameter, one defines the parameters of the halo profile: ρ_s and r_s.

For halos of fixed mass, the concentration is a stochastic variable, with a log-normal probability distribution function:

$$p(c|m,z)dc = \frac{1}{\sqrt{2\pi}\sigma_{\ln c}} \exp\left[-\frac{\ln^2[c/\bar{c}(m,z)]}{2\sigma_{\ln c}^2}\right] d\ln c. \quad (19)$$

In such a case, the variance of concentration virtually does not depend on the halo mass ($\sigma_{\ln c} = 0.2$–0.35; see [37]), whereas the mean value of concentration depends on the mass and redshift. This dependence (the term "mass dependence of concentration" is used hereafter) can be either determined by data of simulations or derived analytically; see [33,38,39]. Since the mass dependence follows from the initial power spectrum of matter, the analytical methods seem to be preferable. The changes in mass dependence caused by modifications of shape or normalization of the initial power spectrum can be easily taken into account.

Analytical techniques aimed to study the mass dependences of profile parameters are usually based on the treatment of Ref. [33]. The data of simulations provide some indications of the growth of profile specific density ρ_s with decrease of the halo mass. As was suggested in Ref. [33], this is due to the tendency of less massive but higher inhomogeneities to collapse earlier. It was assumed also that the specific density of the halo, ρ_s, is proportional to the matter density of the Universe, taken for the moment of collapse, i.e.

$$\rho_s = C\Omega_m \rho_{\rm cr}(1 + z_{\rm col})^3, \quad (20)$$

with the proportionality constant C to be determined from simulation.

The collapse time is defined in an *ad hoc* manner. The collapse is assumed to start at some moment of time, "at which half the mass of the halo was first contained in progenitors more massive than some fraction f of the final mass" [40].

With the Press-Schechter formalism, this condition implies

$$\operatorname{erfc}\left\{\frac{\delta_{\rm col}(z_{\rm col}|z) - \delta_{\rm col}(z|z)}{\sqrt{2(\sigma^2(fM|z) - \sigma^2(M|z))}}\right\} = \frac{1}{2}, \quad (21)$$

leading to the equation

$$\delta_{\rm col}(z_{\rm col}|z) = \delta_{\rm col}(z|z) + C'\sqrt{\sigma^2(fM|z) - \sigma^2(M|z)} \simeq \delta_{\rm col}(z|z) + C'\sigma(fM|z), \quad (22)$$

where $\sigma^2(M|z) = \sigma^2(M)(D(z)/D(0))^2$ and $\sigma^2(M) \equiv \sigma^2(M|z=0)$. Here, z is the moment of halo observation, $C' \approx 0.7$, and the term $\sigma^2(M|z)$ was neglected in comparison with $\sigma^2(fM|z)$. The values of C and f ought to be driven from simulation data. In Ref. [33], f was found to be virtually independent of cosmological parameters at ≈ 0.01; meanwhile, the coefficient $C \sim 10^3$ and is strongly determined by the background cosmological model and/or the initial power spectrum.

As far as C and f have been determined, the specific density of the halo, ρ_s, can be estimated by Eqs. (20) and (22) for given halo mass M as well as the other halo parameter, r_s. Since there is no explicit analytical expression for dependence $\delta_{\rm col}(z_{\rm col}|z)$ in such a treatment, it ought to be recomputed for each cosmology. Therefore, the following simplification of Eq. (22) had been proposed in Ref. [38]:

$$\sigma(fM_\Delta|z_{\rm col}) = 1.686, \quad \text{with} \quad f = 0.01. \tag{23}$$

Also, a simple approximation was proposed therein for the concentration: $c_\Delta = K(1+z_{\rm col})/(1+z)$, with K estimated from numerical modeling as $K = 4$.

As was shown in Ref. [39], the above-mentioned estimation of the concentration parameter from power spectra is applicable to CDM cosmology. However, it is not the case for WDM, since wrong dependences follow from it for smaller scales. According to the computer simulations [39,41], for WDM the concentration tends to grow with the mass increase, whereas for CDM the contrary dependence is expected.

Since the power spectrum and mass dependence of concentration share the same behavior of slopes, it was proposed in [39] to replace Eqs. (22) and (23) by the following:

$$\begin{aligned} \sigma_{\rm eff}(M_s|z_{\rm col}) &= C_\sigma^{-1}, \\ \sigma_{\rm eff}(M|z) &= \sigma(M|z)\left(-\frac{d\ln\sigma(M)}{d\ln M}\right), \end{aligned} \tag{24}$$

where $C_\sigma \approx 28$ and the mass M_s is the one confined within the radius $r_{\rm max} = 2.17 r_s$, where the rotational velocity of a particle has a maximum (for the NFW profile). The following estimation has been proposed in Ref. [39] for the concentration:

$$c_\Delta = \left(\frac{\Delta_{\rm vc}(z_{\rm col})\cdot\Omega_m(z)}{\Delta_{\rm vc}(z)\cdot\Omega_m(z_{\rm col})}\right)^{1/3}\frac{1+z_{\rm col}}{1+z}. \tag{25}$$

This approximation has an obvious drawback, as the moment of collapse, $z_{\rm col}$, should be somehow known in advance, namely, by numerical evaluation using the iteration method for (24). Here, we propose to eliminate these computations by altering a few basic assumptions. The specific density of the halo is assumed to be determined primarily by the collapse of a roughly homogeneous central region of the protocloud. The rest of the halo is formed afterwards around this core by the infall of outer shells. The boundary of the core could be defined as the point where the slope of the density profile changes. Since the accurate determination of such a boundary is cumbersome, the mass of the core, M_c, can be estimated as the mass of the halo contained within radius $r_c = \beta r_s$, where β will be estimated below. In other words, the value of the mean internal density of matter within radius r_c corresponds to the density at the moment when dynamical equilibrium is established.

According to these assumptions,

$$M_c = \frac{4}{3}\pi\rho_{\rm vir}(z_{\rm col})r_c^3 = \frac{4}{3}\pi\Delta_{\rm vc}(z_{\rm col})\rho_{\rm cr}(z_{\rm col})\beta^3 r_s^3, \tag{26}$$

where $\rho_{\rm cr}(z_{\rm col})$ denotes the critical density at the moment of $z_{\rm col}$. On the other hand, integration of the density profile (18) within r_c yields

$$M_c = 4\pi\rho_s r_s^3\left[\ln(1+\beta) - \frac{\beta}{1+\beta}\right]. \tag{27}$$

The total mass of the halo is

$$\begin{aligned} M &= 4\pi\rho_s r_s^3\left[\ln(1+c) - \frac{c}{1+c}\right] \\ &= M_c\frac{\ln(1+c) - c/(1+c)}{\ln(1+\beta) - \beta/(1+\beta)}, \end{aligned} \tag{28}$$

where c is halo concentration.

In order to evaluate the specific density of the halo, ρ_s, the condition of collapse (21) should be redefined for the core of protohalo of mass M_c and radius r_c at the observation moment. So, the new condition takes the form

$$\frac{\delta_{\rm col}(z_{\rm col}|z) - \delta_{\rm col}(z|z)}{\sqrt{2(\sigma^2(fM_c|z) - \sigma^2(M_c|z))}} = \text{const}, \tag{29}$$

where $f < 1$. The term $\sigma^2(M)$ in Eq. (22) should not be neglected for accurate estimation of the concentration dependence on the slope and amplitude of the power spectrum (as in [39]). Moreover, it is crucial for the case of WDM, because $\sigma^2(M)$ changes slowly at small values of mass. So, we can rewrite Eq. (22) as a power series in $(1-f)$:

$$\begin{aligned} \delta_{\rm col}(z_{\rm col}|z) \approx \delta_{\rm col}(z|z) + C'\Bigg[&-\frac{d\sigma^2(M_c)}{d\ln M_c}(1-f) \\ &-\frac{1}{2}\frac{d^2\sigma^2(M_c)}{d\ln M_c^2}(1-f)^2 - \cdots\Bigg]^{1/2}\frac{D(z)}{D(0)}. \end{aligned} \tag{30}$$

In the first order, one can obtain

$$\delta_{\rm col}(z_{\rm col}|z) \simeq \delta_{\rm col}(z|z) + g\left[-\frac{d\sigma^2(M_c)}{d\ln M_c}\right]^{1/2}\frac{D(z)}{D(0)}, \tag{31}$$

where g is a constant, the value of which can be drawn from simulations.

To confront Eq. (31) with that of Ref. [39], the approximation $\delta_{\rm col}(z_{\rm col}|z) = \delta_{\rm col}(z_{\rm col}|z_{\rm col})D(z)/D(z_{\rm col}) \simeq 1.686D(z)/D(z_{\rm col})$ is used, and the term $\delta_{\rm col}(z|z)$ is neglected, since for most of the halos $z_{\rm col} \gg z$ and thus $\delta_{\rm col}(z_{\rm col}|z) \gg \delta_{\rm col}(z|z)$. With these assumptions, Eq. (31) is rendered to

$$\frac{D(z_{\rm col})}{D(0)}\sigma_{\rm eff}(M_c) = (\sqrt{2}g/1.686)^{-1},$$
$$\sigma_{\rm eff}(M_c) = \sigma(M_c)\left(-\frac{d\ln\sigma}{d\ln M_c}\right)^{1/2}. \quad (32)$$

The difference between Eqs. (24) and (32) is apparent, namely, the powers of derivatives: 1/2 in (32) versus 1 in (24). Moreover, the values of constants $\sqrt{2}g/1.686$ and C_σ are not necessarily equal, as the masses M_c and M_s are defined by different radii: $r_c = 0.5r_s$ and $r_{\rm max} = 2.17r_s$, respectively. Hereafter, we advocate the use of Eq. (31) as more accurate and rigorously following from the condition of Ref. [33].

At the next step, to estimate the parameters of the density profile of the halo, the critical amplitude $\delta_{\rm col}(z_{\rm col}|z)$ should be linked with the relative density of the virialized perturbation, $\Delta_{\rm vc}(z_{\rm col})$. For this, $x_{\rm vir}$ must be evaluated from Eq. (15) by using the next expression for local curvature:

$$\Omega_f(z_{\rm col}) = \Omega_K - \frac{5}{3}\Omega_m\frac{\delta_{\rm col}(z_{\rm col}|z)}{D(z)} \quad (33)$$

obtained from Eq. (6). Furthermore, the parameter of the halo density profile r_s as a function of M_c can be found by evaluating the critical amplitude $\delta_{\rm col}(z_{\rm col}|z)$ for given mass M_c with (31) along with Eqs. (15) and (33), above-mentioned definitions, and Eq. (26):

$$r_s = \frac{x_{\rm vir}}{\beta}\left(\frac{(M_c/10^{12}h^{-1}M_\odot)}{1.163\Omega_m}\right)^{1/3}, \quad (34)$$

where r_s has dimension Mpc/h and we have taken into account that $4\pi\rho_{\rm cr}(0)/3 \simeq 1.163\times10^{12}M_\odot h^{-1}/({\rm Mpc}/h)^3$. The specific density of the halo, ρ_s, is evaluated from Eq. (27).

As long as the ratio of the mean density of the halo to the specific density is a function of concentration c:

$$\frac{\rho_{\rm halo}}{\rho_s} = \frac{3M}{4\pi r_{\rm vir}^3\rho_s} = \frac{3}{c^3}\left[\ln(1+c) - \frac{c}{1+c}\right], \quad (35)$$

and the concentration is a function of that ratio, the approximation expression for which is given in Ref. [16]:

$$c \simeq \left[\frac{2}{3}\frac{\rho_{\rm halo}}{\rho_s} + \left(\frac{1.1}{2.0}\frac{\rho_{\rm halo}}{\rho_s}\right)^{0.387}\right]^{-1}. \quad (36)$$

It is convenient to express the specific and mean densities of the halo in units of critical density, i.e. $\Delta_{sc} \equiv \rho_s/\rho_{\rm cr}$ and $\Delta_{hc} \equiv \rho_{\rm halo}/\rho_{\rm cr}$, or in units of the mean density of matter, as $\Delta_{sm} \equiv \rho_s/\bar{\rho}_m$ and $\Delta_{hm} \equiv \rho_{\rm halo}/\bar{\rho}_m$ correspondingly. Thus, $\rho_{\rm halo}/\rho_s = \Delta_{hc}/\Delta_{sc} = \Delta_{hm}/\Delta_{sm}$. According to the condition used to define the halo radius $r_{\rm vir}$, one of the values, either Δ_{hc} or Δ_{hm}, should be constant for all halos; meanwhile, either Δ_{sc} or Δ_{sm} is evaluated by formulas:

$$\Delta_{sc} = \frac{\Omega_m}{x_{\rm vir}^3}\frac{H_0^2}{H^2(z)}\frac{\beta^3/3}{\ln(1+\beta)-\beta/(1+\beta)}, \quad (37)$$

$$\Delta_{sm} = \frac{1}{x_{\rm vir}^3}\frac{1}{(1+z)^3}\frac{\beta^3/3}{\ln(1+\beta)-\beta/(1+\beta)}. \quad (38)$$

Then the total halo mass can be simply evaluated by using Eq. (28).

The approximations for dependences of concentration on mass are presented in Fig. 3 for CDM and WDM (for the set of DM particle masses) along with the data of simulations carried out by Ref. [41]. Also, we used the data of the simulations to find the best-fit values for the parameters, $\beta = 0.7$ and $g = 5.4$, and plotted them along with the approximation of the same authors for comparison; see the bottom panel. All calculations were performed for a

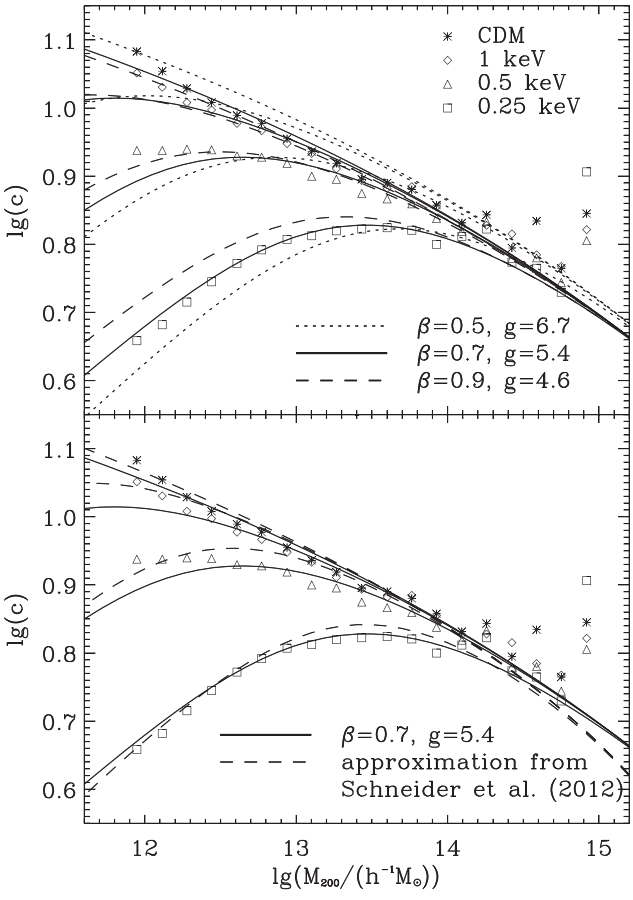

FIG. 3. The dependences of concentration parameter c on halo mass M_{200} for different cosmologies. The data of simulations for CDM (stars) and WDM with different masses of dark matter particles ($m = 1$ keV, diamonds; $m = 0.5$ keV, triangles; $m = 0.25$ keV, squares) are taken from Ref. [41]. Top panel: Our approximation for different parameters, $\beta = 0.5$ and $g = 6.7$, dotted lines; $\beta = 0.7$ and $g = 5.4$, solid lines; and $\beta = 0.9$ and $g = 4.6$, dashed lines. Bottom panel: The comparison of our approximations ($\beta = 0.7$ and $g = 5.4$, solid lines) with approximations in Ref. [41] (dashed lines).

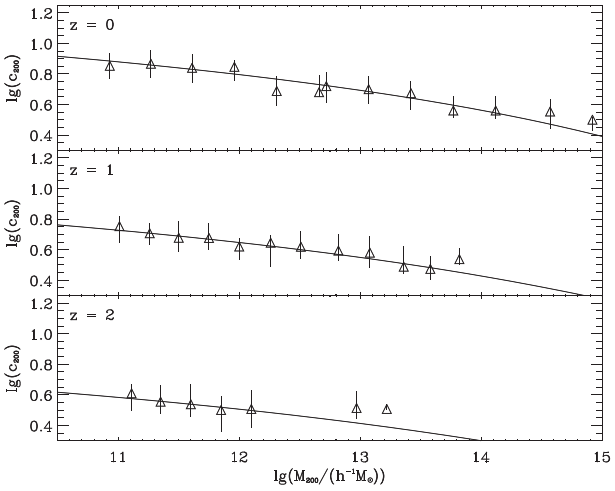

FIG. 4. The dependence of concentration, c_{200}, on the mass M_{200}. The triangles represent the modeling by Ref. [43]. The solid lines represent our results. The plots are given for the redshifts $z = 0$, 1, 2 in downward order.

number of ΛCDM and ΛWDM cosmologies with parameters $\Omega_m = 0.2726$, $\Omega_\Lambda = 0.7274$, $h = 0.704$, $\sigma_8 = 0.809$, and $n_s = 0.963$.

The values of halo concentrations correlate with halo ages, so that the oldest halos are expected to have larger concentrations (see [42] for details). According to hierarchical CDM scenario of clustering, the halos of lower masses should be formed in the first turn, and therefore they should be of larger concentrations. Meanwhile, for the WDM the perturbations at small scales are suppressed by free-streaming. As a result, in the case of WDM the low-mass halos are mainly formed after cooling of warm dark matter caused by expansion of the Universe; hence, they appear to have smaller values of concentration.

Another comparison of our predictions with simulations is presented in Fig. 4, this time with respect to redshift evolution. The evaluated dependence of halo concentration, c_{200}, on mass M_{200}, is presented therein along with the modeling data from Ref. [43], and the parameters of the cosmological model are taken from the 5-year data release of WMAP [44]: $\Omega_\Lambda = 0.721$, $\Omega_m = 0.279$, $\Omega_b = 0.0441$, $h = 0.719$, $\sigma_8 = 0.796$, and $n_s = 0.963$. Three plots represent dependences for the set of redshifts, $z = 0$, 1, 2. Quite good agreement is seen between our calculations and the data of simulations at all redshifts.

IV. MASS FUNCTIONS OF HALOS AND MATTER POWER SPECTRUM

The pioneering paper of Press and Schechter [45] introduced an analytical approach to the statistical description for galaxy cluster distribution. The model of spherical collapse underpins this formalism; the halos are associated with the peaks of an initial Gaussian field of density perturbations. This Press-Schechter formalism utilizes the halo mass function to describe the distribution of halos over masses. The approach was refined and extended afterwards in Refs. [46–48] to allow for the merger histories of dark matter halos. The process of halo merging is assumed to be hierarchical at the large scales and described with a characteristic collapsing mass scale, $m(t_{\rm col})$, complemented with the rms of density perturbations, $\sigma(m) = \delta_{\rm col}(t_{\rm col})$. This mass grows with time through merging of halos and should asymptotically approach in the distant future the limit m_∞ at which $\sigma(m_\infty) = \delta_{\rm min}$, where $\delta_{\rm min}$ is the minimal amplitude of linear density perturbations which can reach the turnaround point followed by collapse and formation of virialized objects for a cosmologically justified time (see for details [29]). For cosmology with $\delta_{\rm min} = 0$, the clustering of dark matter never ends in the sense that all halos of the Universe will merge in the far future.

A. Halo mass function

According to Ref. [46], the Press-Schechter mass function $n(m, z)$, i.e. the number density of gravitationally bound objects with masses m at redshift z, is supposed to satisfy the condition

$$\nu F(\nu) \equiv \frac{m^2 n(m,z)}{\bar\rho_m}\frac{d\ln m}{d\ln \nu} = \sqrt{\frac{\nu}{2\pi}}\exp\{-\nu/2\}, \qquad (39)$$

where $\nu \equiv (\delta_{\rm col}(t_{\rm col})/\sigma(m))^2$ and $\bar\rho_m$ is the background matter density.

The Press-Schechter mass function is proven to be qualitatively correct; however, in some details discrepancies with the data of N-body simulations are found. Therefore, a number of improvements to this approach are proposed. For instance, the treatment of the collapsing perturbations as ellipsoidal rather than spherical diminishes the discrepancies (see [49]). Indeed, by assuming the average ellipticity of perturbation with mass m and amplitude δ to be $e_{mp} = (\sigma(m)/\delta)/\sqrt{5}$, a simple relation was obtained in Ref. [50] to connect ellipsoidal and spherical collapse thresholds:

$$\delta_{\rm ec}(m, t_{\rm col}) = \delta_{\rm col}(t_{\rm col})\left(1 + 0.47\left[\frac{\sigma(m)}{\delta_{\rm col}(t_{\rm col})}\right]^{1.23}\right). \qquad (40)$$

Also, the excursion set model was used in Ref. [46] to estimate the mass function associated with ellipsoidal collapse:

$$\nu F(\nu) = A(p)(1 + \nu^{-p})\sqrt{\frac{\nu}{2\pi}}\exp\{-\nu/2\}, \qquad (41)$$

where parameter $p \simeq 0.3$ and function $A(p) \equiv [1 + 2^{-p}\Gamma(1/2 - p)/\sqrt{\pi}]^{-1} \simeq 0.3222$ are determined by the requirement that the whole mass is gathered within halos, i.e. the integration of $F(\nu)$ over ν yields unity. In order to match the data of GIF numerical simulations, the mass function (41) has been parameterized in Ref. [49] as

$$\nu F(\nu) = A(p)(1 + (q\nu)^{-p})\sqrt{\frac{q\nu}{2\pi}}\exp\{-q\nu/2\}. \quad (42)$$

The additional parameter q was found to be $q = 0.707$, and later it was redetermined in Ref. [51] to be $q = 0.75$. The ellipsoidal threshold for such a mass function, estimated in the framework of the excursion set approach [50], is as follows:

$$\delta_{\rm eq}(m, t_{\rm col}) = q^{\frac{1}{2}}\delta_{\rm col}(t_{\rm col})\left(1 + 0.5\left[\frac{\sigma(m)}{q^{\frac{1}{2}}\delta_{\rm col}(t_{\rm col})}\right]^{1.2}\right). \quad (43)$$

Two different algorithms are commonly used to identify the dark matter halos within the data of numerical N-body simulations: the friend-of-friend (FOF) algorithm [52] and the spherical overdensity (SO) finder [53]. The FOF procedure depends on just one free parameter, b, which defines the linking length as $b\bar{n}^{-1/3}$, where $\bar{n}$ is the average density of particles. Thus, in the limit of a very large number of particles per halo, FOF approximately selects the halo as matter enclosed by an isodensity surface at which $\rho = \bar{\rho}/b^3$. The SO algorithm finds the values of the average halo density in spherical volumes of various sizes. The criterion for halo identification is equality of the average density over the sphere to certain value $\kappa\bar{\rho}_m$, where $\bar{\rho}_m$ is the mean density of matter in the sample and κ is a parameter of the algorithm. For the NFW density profile, these algorithms are not to be identical, as they lead to different mass dependences of the halo concentration parameter c. Nevertheless, the similarity of halo mass functions was found in Ref. [54] by using SO ($\kappa = 180$) and FOF ($b = 0.2$) halo finders.

Hereafter, we refer to the halo as a gravitationally bound system which has reached the state of dynamical equilibrium; meanwhile, both SO and FOF finders select the groups of close particles regardless of their dynamical properties. To divide such halos into virialized (relaxed) and nonvirialized parts, it was suggested in Ref. [55] to assess the dynamical state of each halo processed by the FOF algorithm by means of three objective criteria: (i) the substructure mass function $f_{\rm sub}$, (ii) the center of mass displacement $s = |r_c - r_{\rm cm}|/r_{\rm vir}$, and (iii) the virial ratio $2T/U$. In Ref. [56], the rms of the NFW fit to the density profile has been used, too.

As far as virial density $\rho_{\rm vir} = \rho_{\rm cr}\Delta_{\rm vc} = \bar{\rho}_m\Delta_{vm}$, it seems appropriate to use the SO halo finder with $\kappa = \Delta_{vm} = \Delta_{\rm vc}/\Omega_m$. The equality $\kappa \simeq 180$ is valid for any redshift in flat $\Omega_m = 1$ cosmology (this is close to the $b \simeq 0.2$ for the FOF algorithm); meanwhile, for the ΛCDM cosmology with $\Omega_m = 0.3$, $\Omega_\Lambda = 0.7$, the quantities κ and b depend on redshift: $\kappa \simeq 97/0.3 \simeq 324$ ($b \simeq 0.164$) at $z = 0$ and slowly decrease (increase) to the limit $\kappa \simeq 180$ ($b \simeq 0.2$) at high z. However, as is shown in Ref. [54], the shape of mass function is invariant if we simply identify clusters with a constant linking length $b = 0.2$ for all redshifts and cosmologies.

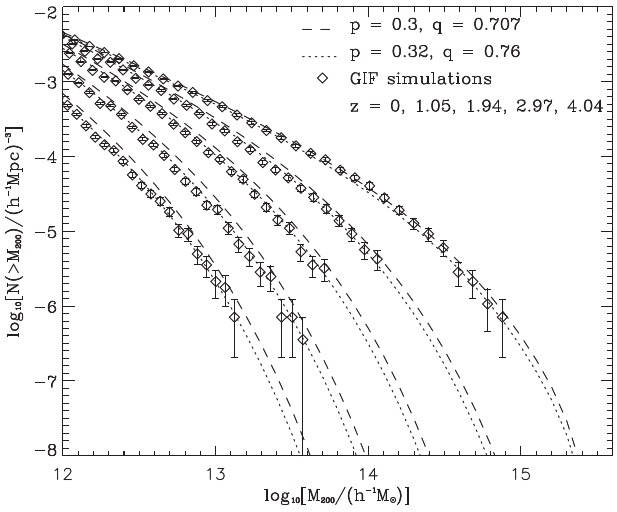

FIG. 5. The halo mass function for different redshifts ($z = 0$, 1.05, 1.94, 2.97, 4.04 from top to bottom). The dashed lines are the Sheth-Tormen approximation with parameters $p = 0.3$ and $q = 0.707$ [49], the dotted lines show the same approximation with modified parameters $p = 0.32$ and $q = 0.76$, and diamonds show results from N-body numerical simulations performed by the GIF/Virgo Collaboration [57].

The halo mass function derived from N-body simulations of the GIF/Virgo Collaboration is plotted in Fig. 5. The catalogs of halos were built from simulations and made available[2]. For each halo detected by the FOF algorithm ($b = 0.2$) the catalogs include the mass M_{200}, confined within the central part of the halo with overdensity $\Delta_{vm} = 200$ (see [57] for details). The mass rescaling slightly affects the observed mass function. We have redetermined the parameters of the Sheth-Tormen approximation to be $p = 0.32$ and $q = 0.76$. As follows from Fig. 5, the refined parameters provide a better fit for the data than the ones from Ref. [49], namely, $p = 0.3$ and $q = 0.707$. The mass function is defined here as a number density of halos with masses exceeding the specified mass m:

$$N(>m) = \int_m^\infty n(m', z)dm' = \int_m^\infty \frac{\bar{\rho}_m}{m'}\nu F(\nu)\frac{d\ln\nu}{dm'}dm'. \quad (44)$$

Note that variations in FOF or SO halo finder parameters also alter the total number of detected halos; meanwhile, the mass rescaling influences the shape of the mass function, not the total number of halos.

The Press-Schechter formalism [45] implies that halos are shaped out of regions with initial overdensities $\delta \geq \delta_{\rm col}$, i.e. the collapsed ones. However, this does not prevent the initially lower overdensities $\delta < \delta_{\rm col}$ to reach the value Δ_{vm}. For the nonlinear overdensity $\delta_M = 180$, the corresponding initial amplitude of the density perturbation (in the

[2]http://www.mpa-garching.mpg.de/GIF

units of the critical one) is $q^{\frac{1}{2}} \equiv \bar{\delta}/\delta_{\rm col} \simeq 0.95$, as follows from (12). Thus, the SO algorithm ($\kappa = \Delta_{vm} = \delta_M + 1$) can by chance mark as halos the nonvirialized regions, the initial amplitude of which exceeds $q^{\frac{1}{2}}\delta_{\rm col}$ but is less than $\delta_{\rm col}$ (for spherical overdensities).

It seems reasonable to assume that the elliptical "q threshold" δ_{eq} is directly connected to the spherical q threshold $q^{\frac{1}{2}}\delta_{\rm col}$ through (43) just in the same manner as the elliptical collapse threshold $\delta_{\rm ec}$ is related to the spherical collapse threshold $\delta_{\rm col}$ with (40). However, the estimate obtained above, $q \simeq 0.95^2 \simeq 0.90$ for $\Delta_{vm} = 180$, substantially deviates from $q \simeq 0.75$, estimated by numerical simulations using the FOF ($b = 0.2$) and SO ($\kappa = 180$) algorithms. The large halos are supposed to be close to spherical, so their mass distribution should comply with the Press-Schechter one. More interestingly, when $\delta_{\rm col}$ in (39) is replaced by the spherical q threshold $0.95\delta_{\rm col}$ (0.9ν for ν), a good match to numerical simulations is attained for large ν and therefore large masses. However, the Press-Schechter mass function tends to overestimate the number of halos with smaller masses, because low-mass protohalos are more elliptical and therefore according to (40) need a larger initial amplitude to became a halo.

B. The dark matter power spectrum

A luminous object is determined by clumping of baryon matter, which in turn is tightly governed by the gravitational potential of dark matter. Hence, the observable spatial distribution of galaxies should follow the distribution of dark matter, since the latter dominates by density. So, in order to reconstruct the observable distribution of galaxies, the characteristics of the distribution of dark matter are needed.

1. Two-point correlation function and power spectrum of discrete and continuous distributions

In statistics, the inhomogeneity of spatial distribution is usually described either by the two-point correlation function or by its Fourier transform, the power spectrum. The latter can be directly drawn by the Fourier transformation of relative density fluctuations. In the case of continuous distribution, it is

$$\delta(\vec{r}) = (2\pi)^{\frac{3}{2}} V^{\frac{1}{2}} \int \delta_{\vec{k}} e^{-i\vec{k}\vec{r}} d^3\vec{k} = \frac{(2\pi)^{\frac{3}{2}}}{V^{\frac{1}{2}}} \sum_{\vec{k}} \delta_{\vec{k}} e^{-i\vec{k}\vec{r}}, \quad (45)$$

where V denotes "volume of periodicity" to be properly chosen. The coefficients of (45) are

$$\delta_{\vec{k}} = \frac{1}{(2\pi)^{3/2} V^{1/2}} \int \delta(\vec{r}) e^{i\vec{k}\vec{r}} d^3\vec{r} = \frac{V^{\frac{1}{2}}}{(2\pi)^{\frac{3}{2}}} \sum_{\vec{r}} \delta(\vec{r}) e^{i\vec{k}\vec{r}}. \quad (46)$$

The Fourier amplitude, squared and averaged over the different directions of vector $\vec{k}$, yields the power spectrum $\mathcal{P}(k) = \langle |\delta_{\vec{k}}|^2 \rangle$. The two-point correlation function is readily derived from the given power spectrum:

$$\xi(r) = \langle \delta(\vec{r}\,')\delta(\vec{r}\,' + \vec{r}) \rangle = \frac{(2\pi)^3}{V} \sum_{\vec{k}} \langle |\delta_{\vec{k}}|^2 \rangle e^{i\vec{k}\vec{r}}$$
$$= \int d^3\vec{k} \langle |\delta_{\vec{k}}|^2 \rangle e^{i\vec{k}\vec{r}} = 4\pi \int_0^\infty k^2 dk \mathcal{P}(k) \frac{\sin(kr)}{kr}, \quad (47)$$

as well as variance of the amplitude within the sphere of radius R:

$$\sigma^2(R) = \langle \delta_R^2 \rangle = 4\pi \int k^2 \mathcal{P}(k) W^2(kR) dk$$
$$= \int \Delta^2(k) W^2(kR) d\ln k, \quad (48)$$

where $W(x) = 3(\sin(x) - x\cos(x))/x^3$ is a window function for the sphere and the quantity $\Delta^2(k) = 4\pi k^3 \mathcal{P}(k)$ is a "dimensionless" power spectrum.

The power spectrum is evaluated from the correlation function as

$$\mathcal{P}(k) = \frac{1}{(2\pi)^3} \int d^3\vec{r} e^{-i\vec{k}\vec{r}} \xi(r). \quad (49)$$

The galaxy catalogs (and the data of numerical simulations) involve discrete distributions of objects ("particles"). Thus, Eqs. (45) and (46) should be rewritten with $\rho(\vec{r}) = \sum_i m_i \delta_D(\vec{r} - \vec{r}_i)$, where m_i is the mass of the ith particle and $\delta_D(\vec{r} - \vec{r}_i)$ is the three-dimensional Dirac function,

$$\delta_{\vec{k}} = \frac{1}{(2\pi)^{3/2} \langle m \rangle \bar{n} V^{1/2}} \sum_i m_i e^{-i\vec{k}\vec{r}_i}, \quad (50)$$

$\bar{n}$ is the spatially averaged number density of particles, and $\langle m \rangle = \sum m_i/(\bar{n}V)$ is the mean mass.

The relation of the power spectrum to the correlation function is provided in Ref. [58], where

$$\mathcal{P}(k) = \frac{\langle m^2 \rangle}{(2\pi)^3 \bar{n} \langle m \rangle^2} + \frac{1}{(2\pi)^3} \int d^3\vec{r} e^{-i\vec{k}\vec{r}} \xi(r), \quad (51)$$

with $\langle m^2 \rangle = \sum m_i^2/(\bar{n}V)$. The first term in the right-hand side is a shot noise, denoted henceforth by $\mathcal{P}_{\rm shot}$. It is inherent for discrete distribution and caused by finiteness of the number density of particles $\bar{n}$. At $\bar{n} \to \infty$, i.e. for continuous distribution, Eqs. (49) and (51) converge. The second term in the right-hand side of (51) is denoted henceforth as $\mathcal{P}_\xi(k)$ to emphasize the nonrandom (correlated) nature of distribution. Thus, Eq. (51) can be written in a more compact form as $\mathcal{P}(k) = \mathcal{P}_{\rm shot} + \mathcal{P}_\xi(k)$.

2. Nonlinear power spectrum in the halo model

Within the halo model, the distribution of matter is treated in a mixed, discrete-continuous manner. The distribution of spatially separated halos of different mass is considered, and the distribution of matter within each halo is described by continuous density profile (18). Therefore, the power spectrum is split into two terms:

one to describe the distribution of halos and the second to describe the distribution of matter within an individual halo. The splitting can be derived rigorously by taking into account that Fourier amplitudes of the density perturbations are (see for details Appendix A)

$$\delta_{\vec{k}} = \frac{1}{\bar{\rho}} \int_0^\infty m \cdot n(m) \delta_{\vec{k}}(m) \bar{y}(m, k) dm. \quad (52)$$

The $\bar{\rho} = \bar{\rho}_m^0 / a^3$ is an average matter density at the moment of time determined by scale factor $a = (1 + z)^{-1}$, and $n(m)$ is the number density of halos with mass m in comoving coordinates, estimated with (42).

The function $\bar{y}(m, k)$ is a Fourier transform of density profile (18) expressed explicitly by analytical form

$$\begin{aligned} \bar{y}(m, k) &= \frac{4\pi}{m} \int_0^{r_{\rm vir}/a} \frac{\sin(kR)}{kR} \rho(Ra) R^2 dR \\ &= \frac{4\pi \rho_s r_s^3}{m a^3} \left\{ \left[Si\left(\frac{kr_s}{a}(1 + c)\right) - Si\left(\frac{kr_s}{a}\right) \right] \sin\left(\frac{kr_s}{a}\right) \right. \\ &\quad + \left[Ci\left(\frac{kr_s}{a}(1 + c)\right) - Ci\left(\frac{kr_s}{a}\right) \right] \cos\left(\frac{kr_s}{a}\right) \\ &\quad \left. - \frac{a}{(1 + c) kr_s} \sin\left(c \frac{kr_s}{a}\right) \right\}, \end{aligned} \quad (53)$$

where c is the halo concentration, ρ_s and r_s are parameters of the density profile, and $Si(x)$ and $Ci(x)$ are integral sine and cosine, respectively. The halo profile depends on the physical coordinates, while the power spectrum is associated with comoving coordinates as $R = r/a$. The term $4\pi\rho_s r_s^3/m$ can be expressed via halo concentration parameter c by using Eq. (28).

The power spectrum $\mathcal{P}(k|m, m')$ of the spatial distribution of halos with given masses m and m' is the following:

$$\begin{aligned} \mathcal{P}(k|m, m') &= \frac{1}{2} \langle \delta_{\vec{k}}^*(m) \delta_{\vec{k}}(m') + \delta_{\vec{k}}(m) \delta_{\vec{k}}^*(m') \rangle \\ &= \frac{\delta_{m,m'}}{(2\pi)^3 n(m)} + \mathcal{P}_\xi(k|m, m'), \end{aligned}$$

where $\delta_{m,m'}$ is the Kronecker symbol, $\mathcal{P}_\xi(k|m, m')$ is the Fourier image of the two-point cross-correlation function of the halos, and the angle brackets in the right-hand side denote the averaging over the directions of $\vec{k}$.

After a series of mathematical transformations, we obtain

$$\begin{aligned} \mathcal{P}(k) &= \frac{1}{(2\pi)^3 \bar{\rho}^2} \int_0^\infty m^2 \cdot n(m) |\bar{y}(m, k)|^2 dm \\ &\quad + \frac{1}{\bar{\rho}^2} \int_0^\infty m \cdot n(m) \bar{y}(m, k) dm \\ &\quad \times \int_0^\infty m' \cdot n(m') \bar{y}(m', k) dm' \mathcal{P}_\xi(k|m, m'). \end{aligned} \quad (54)$$

The quantity $n(m)$ is a number density of halos of masses m.

Under the assumption of linearity, the cross-correlation power spectrum can be represented as $\mathcal{P}_\xi(k|m, m') \approx b(m) b(m') \mathcal{P}_{\rm lin}(k)$, where $\mathcal{P}_{\rm lin}(k)$ is the linear power spectrum of spatial distribution of matter and $b(m)$ is the biasing parameter which characterizes the skew between distributions of halos and matter.

The requirement of homogeneity at largest scales imposes that expression (54) has to asymptotically approach zero for small wave numbers k. Nevertheless, the first term in the right-hand side of (54) never diminishes, because the binning of matter into separate halos (a kind of discretization) introduces noise into the procedure. The expression for noise is derived from the first term in (54) by letting the distribution of halo matter be homogeneous and substituting of the Fourier image of profile $\bar{y}(k, m)$ by the window function $W(kR)$, where $R = (3m/(4\pi\bar{\rho}_m))^{1/3}$. After noise elimination the final expression for the power spectrum of spatial distribution of dark matter is the following:

$$\begin{aligned} \mathcal{P}(k) &= \frac{1}{(2\pi)^3} \int_0^\infty \left(\frac{m}{\bar{\rho}}\right)^2 n(m) [|\bar{y}(m, k)|^2 - W^2(kR)] dm \\ &\quad + \left[\int_0^\infty \frac{m}{\bar{\rho}} b_1(m) n(m) \bar{y}(m, k) dm \right]^2 \mathcal{P}_{\rm lin}(k). \end{aligned} \quad (55)$$

In accordance with Ref. [59], the factor $[|\bar{y}(m, k)|^2 - W^2(kR)]$ is used instead of $[\bar{y}(m, k) - W(kR)]^2$, as mentioned in the review [21] on the halo model. It should be stressed that at the quasilinear stage it yields rather small deviations from the numerical simulation[3] because $[|\bar{y}(m, k)|^2 - W^2(kR)] \geq [\bar{y}(m, k) - W(kR)]^2$ at $k \sim 1/R$.

With Eq. (55), the power spectrum of dark matter is computed for the broad range of scales to confront our estimations with the results of Large Box and GIF2 N-body simulations available from Max Planck Institute for Astrophysics in Garching. The results of the simulation are released as files with coordinates, velocities, and identification numbers of particles. The parameters of simulations, namely, the total number of particles, the size of box, the mass of particles (assumed equal for all particles), and the scale of smoothing are presented in Table I. The latter is introduced in order to eliminate numerical singularities due to particle proximity, when floating-point errors are difficult to control.

To reproduce the structure at small scales, a simulation should engage the high number density of particles. On the other hand, large volume is required to reproduce properly the structure at large scales. A pursuit to simultaneously meet both requirements leads to the huge numbers of particles and consequently to the enormous amount of

[3]At the quasilinear stage, the shape of the power spectrum is still mainly determined by the shape of the initial power spectrum, yet already differs from it (see [60] for details). The halo model tends to underestimate the power at the quasilinear stage [21], in comparison with numerical simulations.

TABLE I. The parameters of Large Box (LB) and GIF2 simulations, available from Max Planck Institute for Astrophysics in Garching (http://www.mpa-garching.mpg.de).

Simulation	Number of particles	L (Mpc/h)	m_p ($M_{\rm sun}$/h)	$l_{\rm soft}$ (Kpc/h)
GIF2	400^3	110.0	1.73×10^9	6.6
LB	512^3	479.0	6.86×10^{10}	30

computational efforts. So, the commonly used trick is to run separate simulations for the largest and smallest scales. The Large Box simulations cover large volumes, whereas the GIF2 simulations provide us with data for small scales with a larger number density of particles.

The power spectrum was evaluated by computation of the sums, $Sr(\vec{k}) = \sum_i \cos(\vec{k}\vec{r}_i)$ and $Si(\vec{k}) = \sum_i \sin(\vec{k}\vec{r}_i)$, followed by overall summation, $\mathcal{P}(\vec{k}) = (Sr^2(\vec{k}) + Si^2(\vec{k}))/((2\pi)^3 \bar{n}^2 V)$. The final power spectrum was estimated by averaging over directions of $\vec{k}$. To eliminate the noise, the power spectrum of homogeneous distribution was computed in advance and substracted later from the total power spectrum.

In Fig. 6, the results are presented for different techniques. The dark matter power spectrum predicted by our halo model, Eq. (55), apparently matches the LB/GIF2 nonlinear power spectrum through all scales up to $k \sim 100$ h/Mpc. Also, the PD96 [61] and HALOFIT [60] approximations are plotted therein, based on the halo model of Hamilton *et al.* [62], as well as scaling relations and fits to numerical simulations. All these approximations appear to properly fit the LB/GIF2 nonlinear power spectrum at the whole range of scales. The linear power spectrum was evaluated by analytical approximation from Ref. [63] (lower solid line in Fig. 6) and normalized to $\sigma_8 = 0.9$.

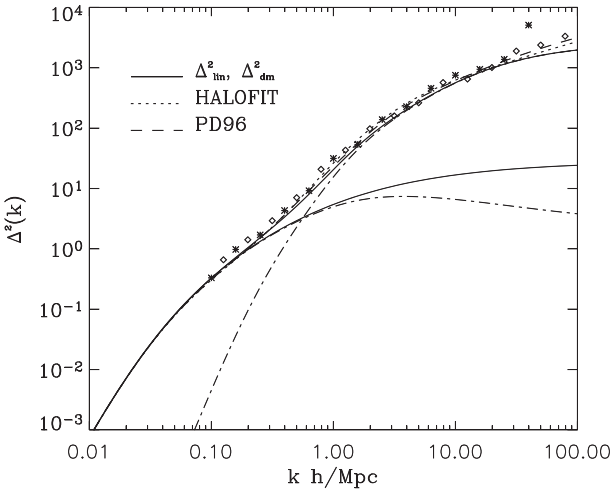

FIG. 6. Dark matter power spectrum from LB (asterisks) and GIF2 (diamonds) simulations. Solid lines represent the primordial linear power spectrum from Ref. [63] (lower line) and our predictions for a nonlinear one (upper line). Dash-dotted lines show the "halo-halo" and the "shot noise" components. Dotted and dashed lines represent PD96 [61] and HALOFIT [60] approximations, respectively. The parameters of the ΛCDM model here are as follows: $(\Omega_m, \Omega_\Lambda, h, \sigma_8, n_s) = (0.3, 0.7, 0.7, 0.9, 1)$.

Since the nonlinear corrections are not essential at $k \leq 0.2$ h/Mpc, the power spectrum appears to be linear there (Fig. 6). The nonlinear clustering enhances the power spectrum at smaller scales, $k > 0.2$ h/Mpc. Both approximations, our (55) and HALOFIT, reproduce such behavior appropriately. The consistency of our estimation with numerical simulation data and the HALOFIT approximation proves the plausibility of our approach.

The halo mass function in WDM cosmology is expected to decline at low masses as $n_h(m) = (1 + m_{hm}/m)^{-0.6} n_{\rm ST}(m)$ [41], where $n_{\rm ST}(m)$ denotes the Sheth-Tormen mass function described in Sec. IV A. The WDM tends to clump less, so that contributes largely to a smooth component of the density field, ρ_s, with $\bar{\rho} = \bar{\rho}_h + \bar{\rho}_s$ [41,64]. To treat the WDM within the framework of the halo model, the separate particles of dark matter are considered as point halos with mass $m_{\rm DM}$, immersed into a smooth component. Thus, the total number density of halos is

$$n(m) = n_h(m) + \frac{\bar{\rho}_s}{m_{\rm DM}} \delta_D(m - m_{\rm DM}). \tag{56}$$

With substitution to (55), similarly to Ref. [64], the power spectrum

$$\mathcal{P}(k) = \frac{1}{(2\pi)^3} \int_0^\infty \left(\frac{m}{\bar{\rho}}\right)^2 n_h(m)[|\bar{y}(m,k)|^2 - W^2(kR)]dm + \left[\int_0^\infty \frac{m}{\bar{\rho}} b_1(m) n_h(m) \bar{y}(m,k) dm + b_s \frac{\bar{\rho}_s}{\bar{\rho}}\right]^2 \mathcal{P}_{\rm lin}(k),$$

where the biasing factor of the smooth component can be obtained from

$$b_s \frac{\bar{\rho}_s}{\bar{\rho}} = 1 - \int_0^\infty \frac{m}{\bar{\rho}} b_1(m) n_h(m) dm.$$

The applicability of these formulas was verified by comparison with the results of numerical simulations from Ref. [65]. The initial distribution of warm dark matter particles for simulation was generated by the following linear power spectrum:

$$\mathcal{P}^{\rm (wdm)}_{\rm lin}(k) = \mathcal{P}^{\rm (cdm)}_{\rm lin}(k)[(1 + (\alpha k)^{2\nu})^{-5/\nu}]^2, \tag{57}$$

with $\nu = 1.12$. The parameter α (in units of Mpc/h) depends on the mass of WDM particles $m_{\rm wdm}$, their density $\Omega_{\rm wdm}$, and Hubble parameter as

$$\alpha(m_{\rm wdm}) = 0.049 \left(\frac{1\ {\rm keV}}{m_{\rm wdm}}\right)^{1.11} \left(\frac{\Omega_{\rm wdm}}{0.25}\right)^{0.11} \left(\frac{h}{0.7}\right)^{1.22}$$

(see also [66,67]).

The nonlinear power spectrum of matter density perturbations at $z = 0.5$ was evaluated by (55) for the

ΛCDM and ΛWDM cosmologies with parameter set $(\Omega_m, \Omega_\Lambda, \Omega_b, h, n_s, \sigma_8) = (0.2711, 0.7289, 0.0451, 0.703, 0.966, 0.809)$ and two masses of warm dark matter particles, $m_{\rm wdm}$, 1 and 0.5 keV, the same as in Ref. [65]. Figure 7 represents the relative discrepancies (percentage) between nonlinear power spectra of cold and warm dark matter (solid lines); also, the corresponding spectra from simulations are plotted along (Fig. 7 in [65]). Our results reveal qualitative consistency with simulations; however, quantitative differences are still noticeable.

It is worth mentioning the discrepancy of halo model and numerical simulations in the case of warm dark matter [68]; see the bottom panels of Fig. 7 in Ref. [65] (green line). That estimation appears to be suppressed in comparison with numerical simulation and seems to be closer to our results. The plausible explanation is that the low-mass halos are more clustered in WDM models than in CDM ones. As was noted in Ref. [69], "formation of low mass halos almost solely within caustic pancakes or ribbons connecting larger halos in a 'cosmic web'" and "voids in this web are almost empty of small halos, in contrast to the situation in CDM theory." This leads to larger values of biasing at $m < m_{hm}$ in WDM models with respect to CDM [41]. We assume that the reason why small halos with mass below m_{hm} are so strongly clustered is that they belong (at least partially) to some larger halos (i.e. they are satellites). Dashed lines in Fig. 7 represent the computations for the case when masses of all halos are increased by 4%, to be above m_{hm}.

Note some aspects of the problem to be addressed in further studies:

(i) The halos with mass $< m_{hm}$ can appear as a result of (i) tidal stripping of dark matter from initially more massive halos, (ii) evaporation of subhalos from large mass halos, and (iii) clustering in the cold component of dark matter.[4] Clarification of the contribution of each such mechanism is needed to update properly the halo model.

(ii) When the power spectra were calculated, the variance of the parameter of halo concentration $\sigma_{\ln c} = 0.25$ was assumed to be the same for cold and warm dark matter and independent of the halo mass. It follows from Fig. 7 that the deviations can be caused by the halo concentration variations.

(iii) The halo model by itself has a number of problems and is not to be considered as ultimately accurate. It is based on some strong assumptions and contains a series of approximations and uncertain statistical procedures and, thus, is prone to systematic errors.

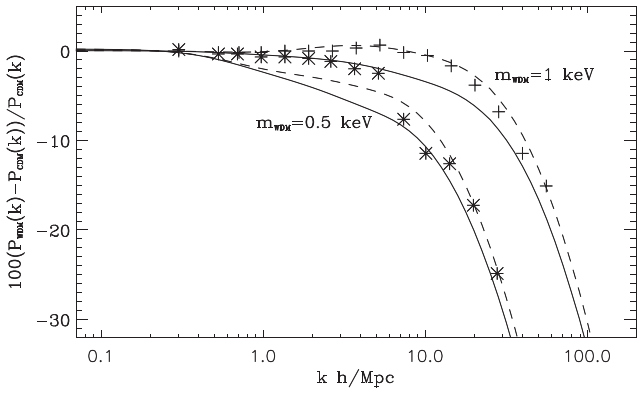

FIG. 7. The difference (percent) between nonlinear power spectra of the ΛCDM and ΛWDM models with $(\Omega_m, \Omega_\Lambda, \Omega_b, h, n_s, \sigma_8) = (0.2711, 0.7289, 0.0451, 0.703, 0.966, 0.809)$ and two values of WDM particle mass: $m_{wdm} = 1$ keV and $m_{wdm} = 0.5$ keV.

C. The galaxy power spectrum

As the baryon gas falls into potential wells of virialized dark matter halos and subhalos, it is heated up to a virial temperature of $T = \frac{1}{2}\mu m_p v_{\rm vir}^2/k_B \approx 2 \times 10^4 \mu_{0.6} (M/10^8 M_\odot)^{2/3}[(1+z)/10]$ K, where $\mu = 0.6\mu_{0.6}$ is the mean molecular mass of postshock gas and M is the mass of halo or subhalo progenitors. The temperature of baryon matter gradually decreases afterwards due to the cooling processes (see [3]). It results in fragmentation to smaller clumps with Bonnor-Ebert mass, $M_{\rm BE} \simeq 700 M_\odot (T/200\ {\rm K})^{3/2}(n_b/10^4\ {\rm cm}^{-3})^{-1/2}$, where n_b is the total number density of baryon particles. At the final stage of this fragmentation, the stars and galaxies are formed (see [2,3] for details). Since formation of galaxies is driven by the gravity of dark matter, the spatial distribution of galaxies should track the spatial distribution of dark matter. In other words, the fluctuations of dark matter density $\delta_{\rm DM}(\vec{r}) = \rho_{\rm DM}(\vec{r})/\bar{\rho}_{\rm DM} - 1$ correlate with fluctuations of galaxy number density $\delta_g(\vec{r}) = n_g(\vec{r})/\bar{n}_g - 1$.

In the halo model, the galaxy number density fluctuations have the following Fourier amplitude:

$$\delta_{g|\vec{k}} = \frac{1}{\bar{n}_g}\int_{m_{\rm min}}^{\infty} \langle N_g|m\rangle n(m)\delta_{\vec{k}}(m)\bar{y}_g(k,m)dm \quad (58)$$

(see Appendix B for details). Here $\langle N_g|m\rangle$ is a mean number of galaxies in the halo with mass m, $\bar{y}_g(k,m)$ is a Fourier transform of the galaxy number density profile, and $m_{\rm min}$ denotes the lowest limit for the halo mass, below which no galaxies are formed. Such a limit naturally stems from degrading efficiency of star formation in halos of low mass [15] and conditions imposed on the sample of galaxies (see [26,27]).

The considerations of the previous subsection are summarized in the following galaxy power spectrum:

[4]The dark matter particles are collisionless, whence part of them, having small velocities, can be considered as cold dark matter.

$$\mathcal{P}_g(k) = \frac{1}{(2\pi)^3}\int_{m_{\min}}^{\infty}\left(\frac{\langle N_g|m\rangle}{\bar{n}_g}\right)^2 n(m)[|\bar{y}_g(m,k)|^2 - W^2(kR_g)]dm + \left[\int_{m_{\min}}^{\infty}\frac{\langle N_g|m\rangle}{\bar{n}_g}b_1(m)n(m)\bar{y}_g(m,k)dm\right]^2\mathcal{P}_{\rm lin}(k), \tag{59}$$

where $R_g = (3\langle N_g|m\rangle/(4\pi\bar{n}_g))^{1/3}$. The resulting equation is similar to the corresponding expression for the galaxy power spectrum from Ref. [21]. The difference is caused by elimination of the noise as described above. Also, the term $\langle N_g|m\rangle^2$ has been obtained instead of $\langle N_g(N_g-1)|m\rangle$ in Ref. [21]. For large-mass halos the term $\langle N_g|m\rangle$ is large, and it seems appropriate to assume the probability distribution $p(N_g|m)$ to be one of Poisson. In this case $\langle N_g|m\rangle^2 \approx \langle N_g(N_g-1)|m\rangle$. However, such an approximation is not valid for low-mass halos.

As it has been outlined in Ref. [14], galaxies within a halo usually are disposed around the center (central galaxy) and within each of its subhalos (satellite galaxies). This gives a clue how to find out the distribution of galaxies over the halo and how it is connected to the substructure. Massive halos usually undergo a violent relaxation, so the resulting velocity dispersion does not depend on masses of particles or subhalos. Therefore, for the number density of the satellites within the halo the following equation is appropriate:

$$n_{\rm sg}(r) = \sum_{m\geq m'_{\min}} n_{\rm sh}(m,r) = \sum_{m\geq m'_{\min}} n_0(m)\exp\left\{-\frac{m\Phi(r)}{kT}\right\} = n_g^0\exp\left\{-\frac{3\Phi(r)}{\sigma_v^2}\right\} = \frac{n_g^0}{\rho_s}\rho(r), \tag{60}$$

where $n_{\rm sh}(m,r)$ denotes the dependence of the number density of halo particles (subhalos) of mass m on the radial distance.

As above, we assume that galaxies are formed within subhalos with masses $m \geq m'_{\min}$, where $m'_{\min}$ is less than $m_{\min}$ because subhalos usually lose mass due to tidal deprivation of their outskirts. Baryon matter (stars) is concentrated to the center and more tightly bound; meanwhile, dark matter is stripped off. Thus, a subhalo at the time of observation is apparently a poor tracer of the potential well, which still determines galaxy properties such as stellar mass or luminosity. A better tracer is the subhalo mass at the time when it falls into the host halo or its maximal mass over its history [14,70]. For massive halos with numerous satellites, the presence of the central galaxy can be neglected. In such a case, as follows from (60), the assumption $\bar{y}_g(m,k) \simeq \bar{y}(m,k)$ is correct. This result agrees with Ref. [71], where the spatial distribution of satellites is studied by using SDSS spectroscopic and photometric galaxy catalogs. They found that satellite profiles generally have a universal form well fitted by the NFW approximation.

However, as long as low-mass halos possess a small number of galaxies, slow relaxation can be important as well. As a result, the profile of satellite galaxy number density generally deviates from the profile of dark matter density. However, such a discrepancy is difficult to detect because of large statistical uncertainties in the determination of the profile of the galaxy number density in such halos. Let us note that in this case the presence of a central galaxy could not be discarded.

The spatial number density of the galaxies is a sum of the halo and subhalo number densities: $n_g(\vec{r}) = n_h(\vec{r}) + n_{\rm sh}(\vec{r})$. The spatial fluctuation of galaxy number density can be thereby split into fluctuations of halo and subhalo number densities:

$$\delta_g(\vec{r}) = \frac{n_h(\vec{r}) + n_{\rm sh}(\vec{r})}{\bar{n}_h + \bar{n}_{\rm sh}} - 1 = \frac{1}{\bar{n}_h + \bar{n}_{\rm sh}}[\bar{n}_h\delta_h(\vec{r}) + \bar{n}_{\rm sh}\delta_{\rm sh}(\vec{r})], \tag{61}$$

where as before the overlines denote averaging in space. The corresponding Fourier amplitude takes the form

$$\delta_{g|\vec{k}} = \frac{1}{\bar{n}_h + \bar{n}_{\rm sh}}[\bar{n}_h\delta_{h|\vec{k}} + \bar{n}_{\rm sh}\delta_{{\rm sh}|\vec{k}}] = \frac{1}{\bar{n}_h + \bar{n}_{\rm sh}}\int_{m_{\min}}^{\infty}[1 + \langle N_{\rm sh}|m\rangle\bar{y}_{\rm sh}(k,m)]n(m)\delta_{\vec{k}}(m)dm, \tag{62}$$

where $\langle N_{\rm sh}|m\rangle$ is the average number of subhalos confined within the halo of mass m, virtually the number of satellites. Since the average number of galaxies accounts for a central galaxy and satellites, $\langle N_g|m\rangle = 1 + \langle N_{\rm sh}|m\rangle$. By comparing Eqs. (58) and (62), one obtains

$$\bar{n}_g = \bar{n}_h + \bar{n}_{\rm sh} = \int_{m_{\min}}^{\infty}[1 + \langle N_{\rm sh}|m\rangle]n(m)dm$$

and

$$\bar{y}_g(k,m) = \frac{\langle N_{\rm sh}|m\rangle\bar{y}_{\rm sh}(k,m) + \bar{y}_c(k,m)}{\langle N_{\rm sh}|m\rangle + 1},$$

where $\bar{y}_{\rm sh}(k,m)$ is a Fourier image of the subhalo number density profile; meanwhile, $\bar{y}_c(k,m)$ is a Fourier image of the probability of finding the central galaxy within the halo.

In cases of a strictly central location of "core" galaxies in all halos with masses m, $\bar{y}_c(k,m) = 1$. For a massive halo, $\langle N_{\rm sh}|m\rangle \gg 1$, so $\bar{y}_g(k,m) \simeq \bar{y}_{\rm sh}(k,m)$, whereas for a low-mass halo, $\langle N_{\rm sh}|m\rangle \ll 1$, $\bar{y}_g(k,m) \simeq \bar{y}_c(k,m)$. As follows from Eq. (60) for massive halos, we can assume $\bar{y}_{\rm sh}(k,m) \simeq \bar{y}(k,m)$. For simplicity, let us extend this

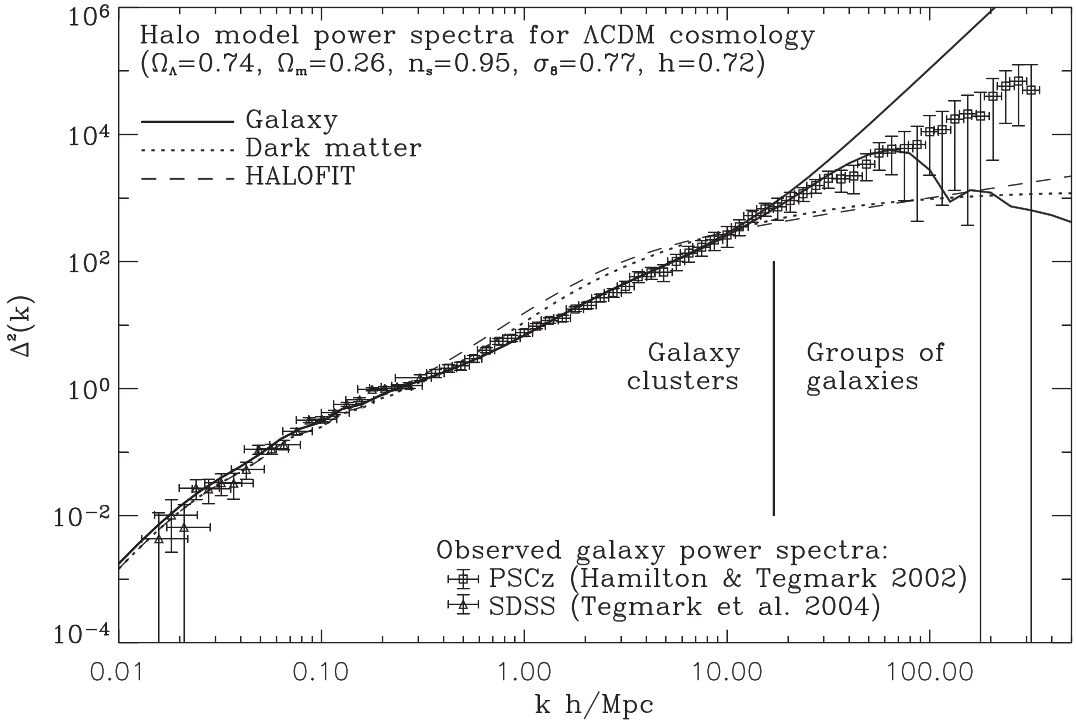

FIG. 8. The power spectra of galaxies (solid line) and dark matter (dotted line) calculated in the halo model for the ΛCDM cosmology with $(\Omega_m, \Omega_\Lambda, h, \sigma_8, n_s) = (0.26, 0.74, 0.72, 0.77, 0.95)$. The squares and triangles represent the observed galaxy power spectrum from the PSCz [26] and SDSS [27] galaxy catalogs, respectively.

approximation to the case of a low-mass halo. It should not bring significant errors to $\bar{y}_g(k, m)$, because in the case of $\langle N_{\rm sh}|m\rangle \ll 1$ the core galaxy is dominating, so $\bar{y}_g(k, m) \simeq \bar{y}_c(k, m)$.

To specify the dependence $\langle N_{\rm sh}|m\rangle$ and to provide a direct link to the galaxy sample, the CLF [11–13] or CMF [14] can be used. The CLF, $\Phi(L|m)dL$, yields the average number of galaxies with luminosity $L \pm dL/2$ which reside within a halo of mass m. The CMF, $\Phi(m_*|m)dm_*$, yields the average number of galaxies with stellar masses in the range $m_* \pm dm_*/2$ which reside within a halo of mass m. The CMF (as well as CLF) can be split into central (core) and satellite parts so that $\Phi(m_*|m) = \Phi_s(m_*|m) + \Phi_c(m_*|m)$. This allows us to calculate the average number of satellites with a stellar masses exceeding m_* within the halo with mass m (see [14] for details):

$$\langle N_{\rm sh}|m, m_*\rangle = \int_{m_*}^{\infty} \Phi_s(m'_*|m)dm'_*,$$

and the probability of finding the appropriate central galaxy is

$$\langle N_c|m, m_*\rangle = \int_{m_*}^{\infty} \Phi_c(m'_*|m)dm'_*,$$

where the upper limit is assigned to infinity, although it actually does not exceed the halo mass m. To calculate the power spectrum of galaxies, we assume that $\langle N_g|m\rangle = \langle N_{\rm sh}|m, m_*\rangle + \langle N_c|m, m_*\rangle$ and

$$\bar{y}_g(k, m) = \frac{\langle N_{\rm sh}|m, m^*\rangle \bar{y}_{\rm sh}(k, m) + \langle N_c|m, m^*\rangle \bar{y}_c(k, m)}{\langle N_{\rm sh}|m, m^*\rangle + \langle N_c|m, m^*\rangle}. \tag{63}$$

The average number of galaxies with a stellar mass larger than m_* is given by

$$\bar{n}_g = \int_0^{\infty} [\langle N_{\rm sh}|m, m_*\rangle + \langle N_c|m, m_*\rangle] n(m)dm. \tag{64}$$

Similar calculations are valid for CLF. Hence, the halo model describes the connection between galaxy power spectrum and stellar masses or luminosities of the sample of galaxies.

Note that our approach differs from the one proposed in Ref. [21], since it allows one to consider the displacements of position of a central galaxy in halos. This is important for small-mass halos which tend to have large ellipticity and shallow potential wells. So, we predict that halos which contain a single galaxy give a contribution to the 1st term of galaxy power spectrum (59), also called a one-halo term.

To prove our approach, we calculate the galaxy power spectrum along with error bars by using the CMF from Ref. [14] for the ΛCDM cosmology with parameters

$(\Omega_m, \Omega_\Lambda, h, \sigma_8, n_s) = (0.26, 0.74, 0.72, 0.77, 0.95)$. The initial dark matter power spectrum $\mathcal{P}_{\rm lin}(k)$ was computed with the CAMB code [72,73] for $\Omega_b = 0.05$. The galaxy power spectrum was evaluated by Eq. (63) and (59) with $W(kR_g)$ replaced by

$$\lim_{\mathcal{P}(k)\to 0} \bar{y}_g(k,m) = \frac{\langle N_{\rm sh}|m,m^*\rangle W(kR_s) + \langle N_c|m,m^*\rangle W(kR_c)}{\langle N_{\rm sh}|m,m^*\rangle + \langle N_c|m,m^*\rangle},$$

where $R_s = (3\langle N_{\rm sh}|m,m^*\rangle/(4\pi\bar{n}_g))^{1/3}$ and $R_c = (3\langle N_c|m, m^*\rangle/(4\pi\bar{n}_g))^{1/3}$. Also, it is assumed that

$$\bar{y}_{\rm sh}(k,m) = \int_{\rm allc} \bar{y}(k, r_s, c')p(c'|m,z)dc', \qquad (65)$$

where $\bar{y}(k, r_s, c)$ denotes the dependence (53) and $p(c|m,z)$ is the probability distribution function for concentration (19) with variance $\sigma_{\ln c} = 0.25$.

The obtained galaxy and dark matter power spectra are presented in Fig. 8 along with observed galaxy power spectra from the PSCz [26] and SDSS [27] galaxy catalogs.

The upper solid line represents the assumption that the core galaxies in all halos with masses m are located strictly in their centers, so $\bar{y}_c(k,m) = 1$. The lower solid line represents the result for the assumption that central galaxies are homogeneously distributed over the spherical volume of radius $1.1r_s$, so $\bar{y}_c(k,m) = W(1.1r_sk)$. We define the lower limit on the stellar masses of the galaxies to be $m_* = 5\times 10^6 M_\odot$.

Thus, at large scales, $k \le 1$ h/Mpc, the dark matter and galaxy power spectra coincide, and at galaxy cluster scales, $1 \le k \le 20$ h/Mpc, they are close and start to diverge at smaller scales, $k > 20$ h/Mpc, where luminous matter is substantially more clustered than dark matter.

V. CONCLUSIONS

The presented semianalytical treatment is our implementation of the halo model, and it is proven to be correct in describing and interpretation of the clustering of the matter at the nonlinear stage of evolution, in both simulation and the observed Universe. Some of the basic elements of the theory are reviewed and improved to calculate the dark matter and galaxy power spectra.

A new technique is proposed for calculating halo concentration parameter c, with phenomenology of halo merging, density profiles, and statistical properties taken into account. The simple expression for estimation (36) depends on the relation of the halo overdensity, Δ_{hc} or Δ_{hm}, and corresponding characteristic halo overdensity, Δ_{sc} or Δ_{sm}, respectively. This relation is evaluated without computing redshift of halo collapse, $z_{\rm col}$, by a set of equations: (16), (31), (33), (36), and (37) or (38) as well. Such a technique has been applied to calculate the concentration parameter for the ΛCDM and ΛWDM cosmological models, and the concordance with data of simulations [39,43] for a vast range of halo masses (Figs. 3 and 4) has been revealed.

The parameters of the Sheth-Tormen approximation for the halo mass function were reevaluated as $p = 0.32$ and $q = 0.76$ (see Fig. 5) to provide the best fit to the data of GIF/Virgo N-body simulations [57] (see Fig. 5).

This modified and extended halo model enables one to predict the dark matter and galaxy power spectra at small scales up to $k \sim 100$ h/Mpc by means of semianalytical methods: Eqs. (54), (55), and (59). The estimated spectra agree with nonlinear power spectra determined from Large Box and GIF2 N-body simulations (Fig. 6) as well as with estimations by galaxy catalogs PSCz [26] and SDSS [27] (Fig. 8). Moreover, with the assumption on the presence of the central galaxies in all halos with masses m [$\bar{y}_c(k,m) = 1$], the technique predicts a galaxy power spectrum matching well the observational one up to $k \sim 20$ h/Mpc. Meanwhile, when the noncentral position of most massive galaxies in halos is assumed [$\bar{y}_c(k,m) = W(1.1r_sk)$], the predictions agree with the observational data up to $k \sim 80$ h/Mpc.

The calculated nonlinear galaxy power spectrum for the ΛCDM cosmology with $(\Omega_m, \Omega_\Lambda, h, \sigma_8, n_s) = (0.26, 0.74, 0.72, 0.77, 0.95)$ corresponds to the observational one for lower limitation on the stellar masses of the galaxies $m_* = 5\times 10^6 M_\odot$. To attain the same level of agreement of the predicted galaxy power spectrum with extracted from galaxy surveys at smaller scales ($k >$ 80 h/Mpc), a new, much more complicated approach for the formation of groups of galaxies should be elaborated.

Despite the ambiguities in the definition of halo, determining of their mass, concentration, and substructure, the halo model provides a good reproduction of such characteristics of large-scale structure of the Universe as the power spectrum and correlation function of the spatial distribution of dark matter and galaxies. In this paper, we have shown how the relation between statistics of the dark matter clustering obtained from numerical simulations and galaxy statistics obtained from large galaxy surveys allows one to calculate the power spectrum of the spatial distribution of the galaxies.

ACKNOWLEDGMENTS

This work was supported by the project of Ministry of Education and Science of Ukraine (state registration No. 0113U003059), research program "Scientific cosmic research" of the National Academy of Sciences of Ukraine (state registration No. 0113U002301), and the SCOPES Project No. IZ73Z0128040 of the Swiss National Science Foundation. Authors also thank to A. Boyarsky and anonymous referees for useful comments and suggestions.

APPENDIX A: FOURIER MODES OF DARK MATTER DENSITY INHOMOGENEITIES

The power spectrum can be derived in a more rigorous manner by the series of following mathematical transformations:

$$\begin{aligned}\delta_{\vec{k}} &= \frac{1}{(2\pi)^{\frac{3}{2}}V^{\frac{1}{2}}}\int_V \delta(\vec{r})e^{i\vec{k}\,\vec{r}}d^3\vec{r} = \frac{1}{(2\pi)^{\frac{3}{2}}V^{\frac{1}{2}}}\sum_i e^{i\vec{k}\vec{r}_i}\int_{V_i}\frac{\rho(\vec{r}-\vec{r}_i)}{\bar{\rho}}e^{i\vec{k}(\vec{r}-\vec{r}_i)}d^3(\vec{r}-\vec{r}_i)\\ &= \frac{1}{(2\pi)^{\frac{3}{2}}\bar{\rho}V^{\frac{1}{2}}}\sum_i e^{i\vec{k}\vec{r}_i}m_i\left\{\frac{1}{m_i}\int_{V_i}\rho(\vec{r}-\vec{r}_i)e^{i\vec{k}(\vec{r}-\vec{r}_i)}d^3(\vec{r}-\vec{r}_i)\right\} = \frac{1}{(2\pi)^{\frac{3}{2}}\bar{\rho}V^{\frac{1}{2}}}\sum_i e^{i\vec{k}\vec{r}_i}m_i y_i(k)\\ &= \frac{1}{\bar{\rho}}\sum_j n(m_j)m_j\left\{\frac{1}{(2\pi)^{\frac{3}{2}}V^{\frac{1}{2}}n(m_j)}\sum_{l=1}^{N_j}e^{i\vec{k}\vec{r}_l}y_l(k,m_j)\right\} = \frac{1}{\bar{\rho}}\int_0^\infty m\cdot n(m)\delta_{\vec{k}}(m)\bar{y}(m,k)dm.\end{aligned}$$

Here, the integration over the whole volume V has been split into integrations over volumes V_i, each occupied by spatially separated halos; the Fourier transform of the ith density profile we denote as $y_i(k)$—it is normalized by its masses m_i. The halos are binned into subsets with equal masses m_j, and the number of halos is denoted by N_j. Also, it was assumed that the halos of equal masses have identical density profiles and, correspondingly, their Fourier transforms, $\bar{y}(m,k)$, are identical, too. $\delta_{\vec{k}}(m)$ is a denotation of the Fourier amplitude of the spatial distribution of halos with masses m. The summation has been changed to the integration.

APPENDIX B: FOURIER MODES OF GALAXY NUMBER DENSITY INHOMOGENEITIES

The Fourier amplitude for relative fluctuations of galaxy concentration takes the following form:

$$\begin{aligned}\delta_{g|\vec{k}} &= \frac{1}{(2\pi)^{\frac{3}{2}}V^{\frac{1}{2}}}\int_V \delta_g(\vec{r})e^{i\vec{k}\,\vec{r}}d^3\vec{r}\\ &= \frac{1}{(2\pi)^{\frac{3}{2}}V^{\frac{1}{2}}}\sum_i e^{i\vec{k}\vec{r}_i}\int_{V_i}\frac{n_g(\vec{r}-\vec{r}_i)}{\bar{n}_g}e^{i\vec{k}(\vec{r}-\vec{r}_i)}d^3(\vec{r}-\vec{r}_i) = \frac{1}{(2\pi)^{\frac{3}{2}}\bar{n}_g V^{\frac{1}{2}}}\sum_i e^{i\vec{k}\vec{r}_i}N_{g|i}\left\{\frac{1}{N_{g|i}}\int_{V_i}n_g(\vec{r}-\vec{r}_i)e^{i\vec{k}(\vec{r}-\vec{r}_i)}d^3(\vec{r}-\vec{r}_i)\right\}\\ &= \frac{1}{(2\pi)^{\frac{3}{2}}\bar{n}_g V^{\frac{1}{2}}}\sum_i e^{i\vec{k}\vec{r}_i}N_{g|i}y_{g|i}(k) = \frac{1}{(2\pi)^{\frac{3}{2}}\bar{n}_g V^{\frac{1}{2}}}\sum_m\sum_{j_m}e^{i\vec{k}\vec{r}_{j_m}}N_{g|j_m}y_{g|j_m}(k,m)\\ &= \frac{1}{\bar{n}_g}\sum_m\bar{y}_g(k,m)\left\{\frac{1}{(2\pi)^{\frac{3}{2}}V^{\frac{1}{2}}}\sum_{j_m}N_{g|j_m}e^{i\vec{k}\vec{r}_{j_m}}\right\} = \frac{1}{\bar{n}_g}\sum_m\bar{y}_g(k,m)\sum_{N=0}^\infty Nn(m,N)\left\{\frac{1}{(2\pi)^{\frac{3}{2}}V^{\frac{1}{2}}n(m,N)}\sum_{l_{mN}}e^{i\vec{k}\vec{r}_{l_{mN}}}\right\}\\ &= \frac{1}{\bar{n}_g}\sum_m\bar{y}_g(k,m)\sum_{N=0}^\infty Nn(m)p(N|m)\delta_{\vec{k}}(m,N) = \frac{1}{\bar{n}_g}\sum_m n(m)\delta_{\vec{k}}(m)\bar{y}_g(k,m)\sum_{N=0}^\infty Np(N|m)\\ &= \frac{1}{\bar{n}_g}\int_0^\infty\langle N|m\rangle n(m)\delta_{\vec{k}}(m)\bar{y}_g(k,m)dm.\end{aligned}$$

Here, as in Appendix A, the integration over the whole volume V was replaced by integration over the number of volumes V_i, filled by spatially separated halos. The Fourier images of profiles of the concentration of galaxies in the halo are normalized by their number $N_{g|i}$; the Fourier image of the ith profile of galaxy concentration is denoted by $y_{g|i}(k)$. The halo was partitioned into subsets of equal masses m and normalized by means of index j_m.

It was assumed that halos of equal masses have identical profiles of galaxy concentration, so their Fourier images $\bar{y}_g(m,k)$ are identical; the sets of halos with equal masses m were partitioned into subsets containing the same number N of galaxies and denoted as $n(m,N)$. The halo concentration $n(m,N)$ is represented as a product of concentration of all halos with mass m and the conditional probability of an event that these halos contain N galaxies each, $n(m,N) = n(m)p(N|m)$. The designation was introduced for the Fourier amplitude of the spatial distribution of halos with masses m and containing N galaxies as $\delta_{\vec{k}}(m,N)$. It was assumed that the spatial distribution of halos of mass m and number of galaxies N matches the spatial distribution of all halos with masses m, $\delta_{\vec{k}}(m) = \delta_{\vec{k}}(m,N)$. The average number of galaxies in a halo of mass m is denoted as $\langle N|m\rangle = \sum_{N=0}^\infty Np(N|m)$, and also the sum was replaced by integration.

[1] S. D. M. White and M. Rees, Mon. Not. R. Astron. Soc. **183**, 341 (1978).
[2] A. Benson, Phys. Rep. **495**, 33 (2010).
[3] C. Safranek-Shrader, V. Bromm, and M. Milosavljevic, Astrophys. J. **723**, 1568 (2010).
[4] N. Katz, D. H. Weinberg, and L. Hernquist, Astrophys. J. Suppl. Ser. **105**, 19 (1996).
[5] V. Springel and L. Hernquist, Mon. Not. R. Astron. Soc. **339**, 289 (2003).
[6] G. Kauffmann, S. D. M. White, and B. Guiderdoni, Mon. Not. R. Astron. Soc. **264**, 201 (1993).
[7] S. Cole, A. Aragon-Salamanca, C. S. Frenk, J. F. Navarro, and S. E. Zepf, Mon. Not. R. Astron. Soc. **271**, 781 (1994).
[8] R. S. Somerville and J. R. Primack, Mon. Not. R. Astron. Soc. **310**, 1087 (1999).
[9] D. J. Croton, V. Springel, S. D. M. White, G. De Lucia, C. S. Frenk, L. Gao, A. Jenkins, G. Kauffmann, J. F. Navarro, and N. Yoshida, Mon. Not. R. Astron. Soc. **365**, 11 (2006).
[10] R. G. Bower, A. J. Benson, R. Malbon, J. C. Helly, C. S. Frenk, C. M. Baugh, S. Cole, and C. G. Lacey, Mon. Not. R. Astron. Soc. **370**, 645 (2006).
[11] X. Yang, H. Mo, and F. van den Bosch, Mon. Not. R. Astron. Soc. **339**, 1057 (2003).
[12] X. Yang, H. J. Mo, Y. P. Jing, F. C. van den Bosch, and Y. Chu, Mon. Not. R. Astron. Soc. **350**, 1153 (2004).
[13] F. C. van den Bosch, X. Yang, H. J. Mo, S. M. Weinmann, A. V. Maccio, S. More, M. Cacciato, R. Skibba, and X. Kang, Mon. Not. R. Astron. Soc. **376**, 841 (2007).
[14] B. Moster, R. S. Somerville, C. Maulbetsch, F. C. van den Bosch, A. V. Macciò, T. Naab, and L. Oser, Astrophys. J. **710**, 903 (2010).
[15] Q. Guo, S. White, C. Li, and M. Boylan-Kolchin, Mon. Not. R. Astron. Soc. **404**, 1111 (2010).
[16] J. A. Peacock and R. E. Smith, Mon. Not. R. Astron. Soc. **318**, 1144 (2000).
[17] C.-P. Ma and J. N. Fry, Astrophys. J. **531**, L87 (2000).
[18] U. Seljak, Mon. Not. R. Astron. Soc. **318**, 203 (2000).
[19] A. A. Berlind and D. H. Weinberg, Astrophys. J. **575**, 587 (2002).
[20] R. Scoccimarro, R. K. Sheth, L. Hui, and B. Jain, Astrophys. J. **546**, 20 (2001).
[21] A. Cooray and R. Sheth, Phys. Rep. **372**, 1 (2002).
[22] C. Giocoli, M. Bartelmann, R. K. Sheth, and M. Cacciato, Mon. Not. R. Astron. Soc. **408**, 300 (2010).
[23] R. K. Sheth and B. Jain, Mon. Not. R. Astron. Soc. **345**, 529 (2003).
[24] R. E. Smith and P. I. R. Watts, Mon. Not. R. Astron. Soc. **360**, 203 (2005).
[25] R. E. Smith, P. I. R. Watts, and R. K. Sheth, Mon. Not. R. Astron. Soc. **365**, 214 (2006).
[26] A. J. S. Hamilton and M. Tegmark, Mon. Not. R. Astron. Soc. **330**, 506 (2002).
[27] M. Tegmark *et al.*, Astrophys. J. **606**, 702 (2004).
[28] R. C. Tolman, *Relativity, Thermodynamics and Cosmology* (Clarendon, Oxford, 1969).
[29] Yu. Kulinich, Kinematics and Physics of Celestial Bodies **24**, 121 (2008).
[30] Yu. Kulinich, B. Novosyadlyj, and V. Pelykh, J. Phys. Stud. **11**, 473 (2007).
[31] Y. Kulinich and B. Novosyadlyj, J. Phys. Stud. **7**, 234 (2003).
[32] P. J. E. Peebles, *The Large-Scale Structure of the Universe* (Princeton University, Princeton, NJ, 1980).
[33] J. Navarro, C. Frenk, and S. White, Astrophys. J. **490**, 493 (1997).
[34] F. Bernardeau, Astron. Astrophys. **291**, 697 (1994).
[35] R. K. Sheth, Mon. Not. R. Astron. Soc. **300**, 1057 (1998).
[36] G. M. Voit, Rev. Mod. Phys. **77**, 207 (2005).
[37] Y. P. Jing, Astrophys. J. **535**, 30 (2000).
[38] J. S. Bullock, T. S. Kolatt, Y. Sigad, R. S. Somerville, A. V. Kravtsov, A. A. Klypin, J. R. Primack, and A. Dekel, Mon. Not. R. Astron. Soc. **321**, 559 (2001).
[39] V. Eke, J. Navarro, and M. Steinmetz, Astrophys. J. **554**, 114 (2001).
[40] V. R. Eke, S. Cole, and C. S. Frenk, Mon. Not. R. Astron. Soc. **282**, 263 (1996).
[41] A. Schneider, R. E. Smith, A. V. Maccio, and B. Moore, Mon. Not. R. Astron. Soc. **424**, 684 (2012).
[42] D. H. Zhao, Y. P. Jing, H. J. Mo, and G. Borner, Astrophys. J. **707**, 354 (2009).
[43] A. Duffy, J. Schaye, S. Kay, and V. Dalla, Mon. Not. R. Astron. Soc. Lett. **390**, L64 (2008).
[44] E. Komatsu *et al.*, Astrophys. J. Suppl. Ser. **180**, 330 (2009).
[45] W. H. Press and P. Schechter, Astrophys. J. **187**, 425 (1974).
[46] J. Bond, S. Cole, G. Efstathiou, and N. Kaiser, Astrophys. J. **379**, 440 (1991).
[47] R. G. Bower, Mon. Not. R. Astron. Soc. **248**, 332 (1991).
[48] C. Lacey and S. Cole, Mon. Not. R. Astron. Soc. **262**, 627 (1993).
[49] R. K. Sheth and G. Tormen, Mon. Not. R. Astron. Soc. **308**, 119 (1999).
[50] R. Sheth, H. Mo, and G. Tormen, Mon. Not. R. Astron. Soc. **323**, 1 (2001).
[51] W. Hu and A. V. Kravtsov, Astrophys. J. **584**, 702 (2003).
[52] M. Davis, G. Efstathiou, C. S. Frenk, and S. D. M. White, Astrophys. J. **292**, 371 (1985).
[53] C. Lacey and S. Cole, Mon. Not. R. Astron. Soc. **271**, 676 (1994).
[54] A. Jenkins, C. S. Frenk, S. D. M. White, J. M. Colberg, S. Cole, A. E. Evrard, H. M. P. Couchman, and N. Yoshida, Mon. Not. R. Astron. Soc. **321**, 372 (2001).
[55] A. F. Neto, L. Gao, P. Bett, S. Cole, J. F. Navarro, C. S. Frenk, S. D. M. White, V. Springel, and A. Jenkins, Mon. Not. R. Astron. Soc. **381**, 1450 (2007).
[56] A. Maccio, A. Dutton, and F. van den Bosch, Mon. Not. R. Astron. Soc. **391**, 1940 (2008).
[57] G. Kauffmann, J. M. Colberg, A. Diaferio, and S. D. M. White, Mon. Not. R. Astron. Soc. **303**, 188 (1999).
[58] P. J. E. Peebles, *Principles of Physical Cosmology* (Princeton University, Princeton, NJ, 1993).
[59] P. Valageas and T. Nishimichi, Astron. Astrophys. **527**, A87 (2011).
[60] R. E. Smith, J. A. Peacock, A. Jenkins, S. D. M. White, C. S. Frenk, F. R. Pearce, P. A. Thomas, G. Efstathiou, and H. M. P. Couchman, Mon. Not. R. Astron. Soc. **341**, 1311 (2003).
[61] J. Peacock and S. Dodds, Mon. Not. R. Astron. Soc. **280**, L19 (1996).
[62] A. J. S. Hamilton, P. Kumar, E. Lu, and A. Matthews, Astrophys. J. **374**, L1 (1991).

[63] G. Efstathiou, J. R. Bond, and S. D. M. White, Mon. Not. R. Astron. Soc. **258**, 1 (1992).
[64] R. E. Smith and K. Markovic, Phys. Rev. D **84**, 063507 (2011).
[65] M. Viel, K. Marković, M. Baldi, and J. Weller, Mon. Not. R. Astron. Soc. **421**, 50 (2012).
[66] S. H. Hansen, J. Lesgourgues, S. Pastor, and J. Silk, Mon. Not. R. Astron. Soc. **333**, 544 (2002).
[67] M. Viel, J. Lesgourgues, M. G. Haehnelt, S. Matarrese, and A. Riotto, Phys. Rev. D **71**, 063534 (2005).
[68] R. E. Smith and K. Marković, Phys. Rev. D **84**, 063507 (2011).
[69] P. Bode, J. P. Ostriker, and N. Turok, Astrophys. J. **556**, 93 (2001).
[70] C. Conroy, R. H. Wechsler, and A. V. Kravtsov, Astrophys. J. **647**, 201 (2006).
[71] Q. Guo, S. Cole, V. Eke, and C. Frenk, Mon. Not. R. Astron. Soc. **427**, 428 (2012).
[72] A. Lewis, A. Challinor, and A. Lasenby, Astrophys. J. **538**, 473 (2000).
[73] http://camb.info.